PHOTO-RHEOLOGY, A NEW METHOD OF EXPERIMENTAL STRESS ANALYSIS FOR ELASTIC-VISCOPLASTIC BODY

Yoshio OHASHI and Tadashi NISHITANI

CONTENTS

Introduction

In the present photo-rheologic method, the viscous strain rate showing time effect is considered besides the instantaneous elastic-plastic strain rate. Therefore, unlike the ordinary photo-plasticity, the strain history dependence which is a property of plastic deformation and the time dependent effect may be accounted in the stress analysis with the use of characteristic values independent of strain rate. Moreover, since the analysis is performed mainly on each element, the method is suitable for analysing the finite deformation.

By using this method, time-dependent deformations and stress states within a body during deformation may be analysed with the same accuracy as photoelasticity, in the process of plastic work or creep deformation.

The fundamental concept and procedure are mentioned in detail with some examples to show the possible application and its distinctive features.

In the conventional photoplasticity for finding the stress distribution in a body subjected to plastic deformation, the body is considered to be in a static equilibrium under external loads, and thus the stress and strain or the optical retardations are considered at such equilibrium state. Therefore, the method may correspond with the so-called deformation theory in plastic analysis. However, since plastic deformation generally depends on the deformation history, the stress-strain relation at a given instant should be considered with a process leading to the final state as well as the state at that time. Thus, the plastic deformation should be characterized generally by a relation between the strain rate, the current stress and its time rate as in the so-called flow theory.

When an inelastic deformation should be considered for real materials, viscosity of the material should be considered in addition to its elastic-plastic property. It is due to the viscosity of the material that a more intensive force is necessary with higher deformation rate for

obtaining the same amount of final deformation.

Photo-rheologic stress analysis mentioned hereafter is a method for finding the stress state in the bodies subjected to plastic work or creep deformation by relating the stress and stress rate in an element of the body to the strain rate which consists of elastic, instantaneous plastic and visous strain rates.

Part I. Fundamental Relations and Experimental Procedures

1. Constitutive Equations of Elastic-Viscoplastic Body

1.1 Loading process [1), 2)]

When the stress increases slowly, the strain rate of an element of a body is considered to consist of the viscous strain rate and the instantaneous elastic-plastic strain rate. When the viscous strain rate is expressed as a form $f(T,t)(\partial F/\partial\sigma_{ij})/2$, the function $f(T,t)$ may be given as

$$f(T,t) = B(t)f_1(T)$$

for the variation of strain which is not so large and complex, where t denotes time, $T^2 = s_{ij}s_{ij}/2$, and s_{ij} denote the components of stress deviator, F is a flow potential, and σ_{ij} denote the components of stress tensor. The above form has been verified experimentally for each value of stress when the relation between creep strain and time is similar for each value of constant stress.

The next forms

$$B(t) = B_0 t^{\alpha}, \quad f_1(T) = e^{bT}$$

are assumed, where B_0, α and b are characteristic values of the material. The former one is that generally used in the creep theory, and the latter holds in a wide range of T and has been verified experimentally to be a good approximation especially for celluloid[3]. T^2 is adopted hereafter as the flow potential.

Ramberg-Osgood's relation

$$2G\dot{e}_{ij} = \dot{s}_{ij} + \frac{2n+1}{2}(T^2/k^2)^n(\dot{T}^2/T^2)s_{ij}$$

may be used as a good approximation of the non-linear stress-strain relation in the elastic-plastic deformation, where G denotes the modulus of rigidity, e_{ij} are the components of strain deviator, n and k are characteristic values, and the dot over the symbol denotes the derivative with respect to time. By using the relation $e_{ij} = \varepsilon_{ij} - e\delta_{ij}$, where e is a mean strain and ε_{ij} are the components of strain tensor, the components of elastic-plastic strain rate $\dot{\varepsilon}_{ij}$ may be expressed as

$$\dot{\varepsilon}_{ij} = \dot{e}\delta_{ij} + \frac{\dot{s}_{ij}}{2G} + \frac{2n+1}{4G}(T^2/k^2)^n(\dot{T}^2/T^2)s_{ij}.$$

As a sum of the above mentioned two parts, components of strain rate ξ_{ij} of the element are expressed as follows:

$$\xi_{ij} = \frac{B_0}{2} - t^{\alpha}e^{bT}\frac{\partial T^2}{\partial\sigma_{ij}} + \dot{e}\delta_{ij} + \frac{\dot{s}_{ij}}{2G} + \frac{2n+1}{4G}(T^2/k^2)^n(\dot{T}^2/T^2)s_{ij}. \tag{1}$$

With the components of principal stress σ_1, σ_2 and σ_3, T^2 is expressed as follows:

$$T^2 = \left\{(\sigma_1-\sigma_2)^2 + (\sigma_2-\sigma_3)^2 + (\sigma_3-\sigma_1)^2\right\}/6. \tag{2}$$

In a calibration test mentioned later, a combined loading of axial stress σ_1 and oil pressure

σ_2 ($\sigma_1 \neq \sigma_2 = \sigma_3$) will be applied to a uni-axial specimen. When the principal stress difference is denoted as $\Delta\sigma = \sigma_1 - \sigma_2$,

$$T^2 = (\Delta\sigma)^2/3, \quad \dot{T}^2 = 2\Delta\sigma\Delta\dot{\sigma}/3 \tag{3a}$$

are obtained from eq. (2). If σ_3 is selected as the principal stress normal to a plane and the incompressibility is assumed,

$$T^2 = (\Delta\sigma)^2/4, \quad \dot{T}^2 = \Delta\sigma\Delta\dot{\sigma}/2 \tag{3b}$$

are obtained for plane strain state. Since $\sigma_3=0$ for the plane stress state, the next relations

$$T^2 = \frac{(\Delta\sigma)^2}{4}\left\{1+\left(\frac{\sigma_0}{\sqrt{3}\Delta\sigma}\right)^2\right\}, \qquad \dot{T}^2 = \frac{\Delta\sigma\Delta\dot{\sigma}}{2}\left\{1+\frac{\sigma_0\dot{\sigma}_0}{3\Delta\sigma\Delta\dot{\sigma}}\right\} \tag{3c}$$

are obtained from eq. (2), where $\sigma_1 + \sigma_2 = \sigma_0$.

By substituting each of eqs. (3) into eq. (1), the principal strain rate difference in each state is expressed by the principal stress difference as follows:

i) State of calibration specimen ($\sigma_1 \neq \sigma_2 = \sigma_3$)

$$\Delta\dot{\varepsilon} = \dot{\xi}_1 - \dot{\xi}_2 = \frac{B_0}{2}t^{\alpha}\Delta\sigma e^{(b/\sqrt{3})\Delta\sigma} + \frac{\Delta\dot{\sigma}}{2G}\left\{1+(2n+1)\left(\frac{\Delta\sigma}{\sqrt{3}k}\right)^{2n}\right\} \tag{4a}$$

ii) Plane strain state

$$\Delta\dot{\varepsilon} = \frac{B_0}{2}t^{\alpha}\Delta\sigma e^{(b/2)\Delta\sigma} + \frac{\Delta\dot{\sigma}}{2G}\left\{1+(2n+1)\left(\frac{\Delta\sigma}{2k}\right)^{2n}\right\} \tag{4b}$$

iii) Plane stress state

$$\Delta\dot{\varepsilon} = \frac{B_0}{2}t^{\alpha}\Delta\sigma\exp\left[\frac{b}{2}\Delta\sigma\left\{1+\left(\frac{\sigma_0}{\sqrt{3}\Delta\sigma}\right)^2\right\}^{1/2}\right] + \frac{\Delta\dot{\sigma}}{2G}\left\{1+(2n+1)\left(\frac{\Delta\sigma}{2k}\right)^{2n}\left\{1+\left(\frac{\sigma_0}{\sqrt{3}\Delta\sigma}\right)^2\right\}^{n-1}\right.$$
$$\left.\times\left(1+\frac{\sigma_0\dot{\sigma}_0}{3\Delta\sigma\Delta\dot{\sigma}}\right)\right\} \tag{4c}$$

Equation (4c) for plane stress state contains the sum of principal stresses and has a complicated form whereas eqs. (4a) and (4b) have relatively simple forms. However, if the value of $\sigma_0/(\sqrt{3}\Delta\sigma)$ in eq. (4c) is sufficiently small in comparing with unity, eq. (4c) may be reduced to the same form as eq. (4b). Thus, eq. (4b) may be used in the plane stress state when the principal stresses have different signs. When either of principal stresses is equal to zero, since $\sigma_0^2 = (\Delta\sigma)^2$ and $1+(\sigma_0/\sqrt{3}\Delta\sigma)^2 = 4/3$ hold, eq. (4c) becomes to a form similar to that of eq. (4a). Thus, eqs. (4a) and (4b) will be considered hereafter.

1.2 Unloading and reversed loading processes

A new coordinate whose axes are taken in opposite direction to those in the preceding coordinate are used at a time t_* of the beginning of unloading, and symbols in this coordinate will be distinguished with the bar over the symbol. The time, principal stresses, strain rate and stress rate are thus expressed as $\bar{t} = t - t_*$, $\bar{\sigma}_{ij}(\bar{t}) = \sigma_{ij}(t) - \sigma_{ij}(t_*)$, $\dot{\bar{\varepsilon}}_{ij}(\bar{t}) = -\dot{\varepsilon}_{ij}(t)$ and $\dot{\bar{\sigma}}_{ij}(\bar{t}) = -\dot{\sigma}_{ij}(t)$, respectively.

In the unloading and succeeding reversed loading processes, the components of strain rate may be expressed in the next form

$$\dot{\xi}_{ij} = \frac{B_1}{2}\bar{t}^{\beta}e^{b'\bar{T}}\frac{\partial\bar{T}^2}{\partial\bar{\sigma}_{ij}} + \dot{\bar{e}}\delta_{ij} + \frac{\dot{\bar{S}}_{ij}}{2G'} + \frac{2n'+1}{4G'}(\bar{T}^2/k'^2)^{n'}(\dot{\bar{T}}^2/\bar{T}^2)\bar{S}_{ij},$$

where B_1, β, b', G', n' and k' are characteristic values in these processes. Since $\overline{T}$ may be expressed with $\overline{\sigma}_1$, $\overline{\sigma}_2$ and $\overline{\sigma}_3$ as in the next form

$$\overline{T}^2=\left\{(\overline{\sigma}_1-\overline{\sigma}_2)^2+(\overline{\sigma}_2-\overline{\sigma}_3)^2+(\overline{\sigma}_3-\overline{\sigma}_1)^2\right\}/6,$$

in the same as the loading process, the principal strain rate difference in the unloading may be expressed as

$$\Delta\dot{\overline{\varepsilon}}(\overline{t})=\frac{B_1}{2}\overline{t}^{\beta}\Delta\overline{\sigma}(t)e^{(b'/\sqrt{3})\Delta\overline{\sigma}t}+\frac{\Delta\dot{\overline{\sigma}}(\overline{t})}{2G'}\left\{1+(2n'+1)\left\{\frac{\Delta\overline{\sigma}(t)}{\sqrt{3}k'}\right\}^{2n'}\right\},$$

$$\Delta\dot{\overline{\varepsilon}}(\overline{t})=\frac{B_1}{2}\overline{t}^{\beta}\Delta\overline{\sigma}(t)e^{(b'/2)\Delta\overline{\sigma}t}+\frac{\Delta\dot{\overline{\sigma}}(\overline{t})}{2G'}\left\{1+(2n'+1)\left\{\frac{\Delta\overline{\sigma}(t)}{2k'}\right\}^{2n'}\right\},$$

which are negative values in the preceding coordinate.

Moreover, since the creep deformation continues to appear for the operating load even in the unloading process, this deformation should be also accounted. In the plastic deformation, the strain state cannot attain immediately to the static equilibrium for the corresponding stress. Accordingly, the stress continues to increase in the loading process while the strain state cannot attain to that of static equilibrium for the corresponding stress. The strain which could not appear in the loading process thus continues to appear in the early stage of unloading. Taking into account this effect, the principal strain rate difference of each element in the body in unloading process may be expressed as follows:

i) Stress state in calibration specimen

$$\Delta\dot{\overline{\varepsilon}}(\overline{t})=\frac{B_1}{2}\overline{t}^{\beta}\Delta\overline{\sigma}(t)e^{(b'/\sqrt{3})\Delta\overline{\sigma}t}+\frac{\Delta\dot{\overline{\sigma}}(\overline{t})}{2G'}\left\{1+(2n'+1)\left\{\frac{\Delta\overline{\sigma}(t)}{\sqrt{3}k'}\right\}^{2n'}\right\}-\frac{B_0'}{2}t^{\alpha}\Delta\sigma(t)e^{(b/\sqrt{3})\Delta\sigma t},\qquad(5a)$$

ii) Plane strain state

$$\Delta\dot{\overline{\varepsilon}}(\overline{t})=\frac{B_1}{2}\overline{t}^{\beta}\Delta\overline{\sigma}(t)e^{(b'/2)\Delta\overline{\sigma}t}+\frac{\Delta\dot{\overline{\sigma}}(\overline{t})}{2G'}\left\{1+(2n'+1)\left\{\frac{\Delta\overline{\sigma}(t)}{2k'}\right\}^{2n'}\right\}-\frac{B_0'}{2}t^{\alpha}\Delta\sigma(t)e^{(b/2)\Delta\sigma t},\qquad(5b)$$

where $B_0'=0$ for $\Delta\sigma(t)<0$.

If the element is subjected only to unloading, as the plastic deformation in the unloading process may be neglected, eq. (5) may be expressed as follows:

i) Stress state in calibration specimen

$$\Delta\dot{\overline{\varepsilon}}(\overline{t})=\frac{B_1}{2}\overline{t}^{\beta}\Delta\overline{\sigma}(t)e^{(b'/\sqrt{3})\Delta\overline{\sigma}t}+\frac{\Delta\dot{\overline{\sigma}}(\overline{t})}{2G'}-\frac{B_0'}{2}t^{\alpha}\Delta\sigma(t)e^{(b/\sqrt{3})\Delta\sigma t},\qquad(6a)$$

ii) Plane strain state

$$\Delta\dot{\overline{\varepsilon}}(\overline{t})=\frac{B_1}{2}\overline{t}^{\beta}\Delta\overline{\sigma}(t)e^{(b'/2)\Delta\overline{\sigma}t}+\frac{\Delta\dot{\overline{\sigma}}(\overline{t})}{2G'}-\frac{B_0'}{2}t^{\alpha}\Delta\sigma(t)e^{(b/2)\Delta\sigma t}.\qquad(6b)$$

2. Optical Effect

When the polarized light is projected normally into a two-dimensional model in a stressed state, the optical vector of light is separated into two components oscillating in the planes containing the principal axes of optical anisotropy induced by the stress. The optical anisotropy appearing in a stressed material, which was initially isotropic, may be considered to consist of two parts. One part is the elastic strain which is the distorsion and change of orientation of molecular chains induced by the stress, and the other is the viscoplastic strain which is the parmanent change of orientation of molecular chains appearing with the flow of material and remains after removal of the stress. Therefore, if the part due to elastic strain is related to the

stress and the rest is related to the viscoplastic strain, the optical retardation would be regarded as a function of the principal stress difference $\Delta\sigma$ and the principal viscoplastic strain difference $\Delta\varepsilon'$. The fringe order per unit thickness $N(t)$ is thus expressed as

$$N(t) = \mathrm{f}\{\Delta\sigma(t),\ \Delta\varepsilon'(t)\}.$$

Since N does not vanish for the stress-free state after plastic deformation, it may be expressed as

$$N = C_1\Delta\sigma\mathrm{f}_1(\Delta\varepsilon') + \mathrm{f}_2(\Delta\varepsilon'),\quad C_1:\mathrm{const.}$$

If the product of principal stress difference and the principal viscoplastic strain difference can be neglected, according to the experimental evidence [3], the above relation is further simplified to

$$N = C_1\Delta\sigma + \mathrm{f}_2(\Delta\varepsilon'). \tag{7}$$

The form of $\mathrm{f}_2(\Delta\varepsilon')$ is selected to approximate as simply and acculately as possible the relation between N and $\Delta\varepsilon'$ obtained by a calibration test under proportional loading. As the result, eq. (7) can be expressed as follows:

$$N(t) = C_1\Delta\sigma(t) + C_2\Delta\varepsilon'(t) + C_3\{\Delta\varepsilon'(t)\}^{3/2} + C_4\{\Delta\varepsilon(t)\}^2 \tag{8}$$

for loading process. In the same manner, the next relation may be obtained for unloading process

$$\overline{N}(t) = N(t) - N(t_*) = C_5\Delta\overline{\sigma}(t) + C_6\Delta\overline{\varepsilon}'(t) + C_7\{\Delta\overline{\varepsilon}'(t)\}^{3/2} + C_8\{\Delta\overline{\varepsilon}'(t)\}^2. \tag{9}$$

Especially, as the plastic strain is not so significant in the unloading, eq. (9) may be simplified as follows:

$$\overline{N}(t) = C_5\Delta\overline{\sigma}(t) + C_6\Delta\overline{\varepsilon}'(t). \tag{10}$$

The coefficients C_1 through C_8 are independent of the state of deformation or principal stress ratio.

In the proportional loading, the values of the principal strain difference are obtained by integrating eqs. (4) through (6) with respect to time and are expressed as follows:

i) Stress state in calibration specimen

$$\Delta\varepsilon(t) = \frac{B_0}{2}\int_0^t \tau^{\alpha}\Delta\sigma(\tau)\mathrm{e}^{\{b/\sqrt{3}\}\Delta\sigma(\tau)}d\tau + [1 + \{\Delta\sigma(t)/\sqrt{3}k\}^{2n}]\Delta\sigma(t)/2G, \tag{11a}$$

ii) Plane strain state

$$\Delta\varepsilon(t) = \frac{B_0}{2}\int_0^t \tau^{\alpha}\Delta\sigma(\tau)\mathrm{e}^{\{b/2\}\Delta\sigma(\tau)}d\tau + [1 + \{\Delta\sigma(t)/2k\}^{2n}]\Delta\sigma(t)/2G \tag{11b}$$

for each element after time t of loading from the initial state, and

i) Stress state in calibration specimen

$$\Delta\overline{\varepsilon}(t) = \frac{B_1}{2}\int_{t*}^t \tau^{\beta}\Delta\overline{\sigma}(\tau)e^{\{b/\sqrt{3}\}\Delta\overline{\sigma}(\tau)}d\tau + [1 + \{\Delta\overline{\sigma}(t)/\sqrt{3}k'\}^{2n'}]\Delta\overline{\sigma}(t)/2G'$$
$$-\frac{B_0'}{2}\int_{t*}^t \tau^{\alpha}\Delta\sigma(\tau)e^{\{b/\sqrt{3}\}\Delta\sigma(\tau)}d\tau, \tag{12a}$$

ii) Plane strain state

$$\Delta\bar{\varepsilon}(t)=\frac{B_1}{2}\int_{t*}^{t}\bar{\tau}^{\beta}\Delta\bar{\sigma}(\tau)e^{(b'/2)\Delta\bar{\sigma}(\tau)}\,d\tau+[1+\{\Delta\bar{\sigma}(t)/2k'\}^{2n'}]\Delta\bar{\sigma}(t)/2G'$$

$$-\frac{B_0'}{2}\int_{t*}^{t}\tau^{\alpha}\Delta\sigma(\tau)e^{(b/2)\Delta\sigma(\tau)}\,d\tau \qquad (12b)$$

for unloading and reversed loading after time t from the beginning of unloading t_*. When the element is subjected only to unloading, the second term in the square bracket in each of eq. (12) may be neglected.

The principal viscoplastic strain difference $\Delta\varepsilon'$ or $\Delta\bar{\varepsilon}'$ related to the fringe order is obtained by subtracting the elastic part $\Delta\sigma(t)/2G$ or $\Delta\bar{\sigma}(t)/2G'$ from eq. (11) or (12).

Calibration tests are performed under proportional loading and thus eqs. (11a) and (12a) represent the strain difference exactly at the final state of loading. For general deformation states, however, the principal directions of stress and strain could vary independently which would result in a slight difference between the principal axes of stress and viscoplastic strain obtained through the deformation history. However, such a difference is not so significant in general and thus, eqs. (11b) and (12b) for the state of plane strain may be regarded as a sufficient approximation in such cases. By using eqs. (11) and (12) with eqs. (8) through (10), $N(t)$ and $\bar{N}(t)$ can thus be expressed as functions of principal stress difference $\Delta\sigma(t)$.

3. *Calibration Test* [2)]

The coefficients of eqs. (4) through (6) are the characteristic values of the material depending on temperature, principal stress ratio and others. As these equations are expressed in terms of time rates, unlike in the photoplasticity, the coefficients are independent of the strain and stress rates and thus, they can be used in analysing the stress state in an elastic-viscoplastic body.

In a calibration test for determining these coefficients, a combined loading of axial stress σ_1 and oil pressure σ_2 is applied to a uniaxial specimen ($\sigma_1 \neq \sigma_2 = \sigma_3$).

3.1 *Apparatus of Calibration Test*

Figure 1 shows an apparatus where a uniaxial specimen is arranged within a vessel Ⓐ and subjected to a combined loading of axial load and oil pressure. A heating unit is also arranged within the vessel for heating the specimen through pressure oil. An axial load is applied with a handle Ⓑ and its magnitude is recorded by an auto-balance type recorder Ⓔ through a load-cell Ⓒ. The oil pressure is applied with a pump Ⓖ and the pressure is regulated with a valve Ⓕ sufficiently precisely and its magnitude is recorded by the same recorder Ⓔ through a pressure gauge Ⓓ using a wire resistance strain gauge.

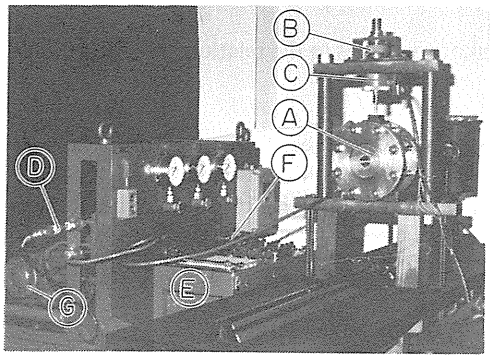

Fig. 1 Apparatus for calibration test

3.2 *Procedure of calibration test*

When a softened celluloid is used as material of model test, as its deformation is sensitive to temperature, the range of temperature distribution around the specimen and its variation during testing should be kept as small as possible. The temperature may be controlled by means

of thermometer of thirmister type with an accuracy of 0.05°C with the use of voltage regulator and on-off type controller.

After the temperature in the vessel Ⓐ is settled as an assigned value, the load is applied to the specimen. Loading rate may be controlled in the following manner. Curves corresponding to the change of axial load and oil pressure are drawn first on a recording sheet of the recorder Ⓔ and the sheet is fed with a constant speed. Then, the axial load and pressure are controlled manually by adjusting the loading handle Ⓑ and the valve Ⓕ so that the recording pens from the load-cell Ⓒ and the pressure gauge Ⓓ may trace the curves.

Since the axial stress is an actual load acting on a unit cross sectional area of the specimen, an effect of area contraction of the specimen should be considered as the specimen is deformed.

σ_1 and σ_2 selected as axial stress and oil pressure are principal stresses. In the following, the principal stress difference $\Delta\sigma=\sigma_1-\sigma_2$ and its time rate $\Delta\dot{\sigma}$ will be mentioned. As there are many combinations of σ_1 and σ_2 for the assigned value of $\Delta\sigma$, the principal stress ratio σ_1/σ_2 should be considered as a parameter.

3.3 Determination of characteristic values

a) Loading process The characteristic values depend on the material, temperature and the principal stress ratio. In a calibration test, loads are applied to a uniaxial celluloid specimen softened at an assigned temperature.

In the case of $\Delta\sigma=a$ (const.) and $\Delta\dot{\sigma}=0$,

$$\Delta\dot{\varepsilon}(t)=\frac{B_0}{2}t^{\alpha}ae^{ab/\sqrt{3}}$$

is obtained from eq. (4a). Taking logarithms of both sides, the next relation is obtained.

$$\log_{10}\{2\Delta\dot{\varepsilon}(t)/a\}=\log_{10}B_0+\alpha\log_{10}t+0.4343\,ab/\sqrt{3}. \tag{13}$$

As the values of $\Delta\dot{\varepsilon}(t)$ and t are known from the experiment, values of B_0, α and b are determined by the experiment for more than two different values of a.

For the case of $\Delta\dot{\sigma}=c$ and $\Delta\sigma=ct$, the following relation is obtained from eq. (11a).

$$\Delta\varepsilon(t)=\frac{B_0}{2}t^{\alpha+1}\Delta\sigma(t)\sum_{m=0}^{\infty}\frac{(b\Delta\sigma(t)/\sqrt{3})^m}{m!(\alpha+m+2)}+\frac{\Delta\sigma(t)}{2G}[1+\{\frac{\Delta\sigma(t)}{\sqrt{3}k}\}^{2n}]. \tag{14}$$

Unknown values in the relation are G, k and n. As the relation

$$\Delta\varepsilon(t)\simeq\Delta\sigma(t)/2G$$

may approximate eq. (14) within a range of small value of t, the value of G may be found from an experiment in this range.

By expressing the known terms in eq. (14) with $A_1(t)$ as

$$A_1(t)=\Delta\varepsilon(t)-\frac{\Delta\sigma(t)}{2G}-\frac{B_0}{2}t^{\alpha+1}\Delta\sigma(t)\sum_{m=0}^{\infty}\frac{(b\Delta\sigma(t)/\sqrt{3})^m}{m!(\alpha+m+2)},$$

eq. (14) may be rewritten as

$$A_1(t)=\frac{\{\Delta\sigma(t)\}^{2n+1}}{2G(\sqrt{3}k)^{2n}}$$

or

$$\log_{10}A_1(t)=(2n+1)\log_{10}\Delta\sigma(t)-\log_{10}2G(\sqrt{3}k)^{2n}. \tag{15}$$

As the values of G, $A_1(t)$ and $\Delta\sigma(t)$ in the relation have been known already, values of k and n

may be found from the experiment. In the calibration test, fringe order per unit thickness $N(t)$ may be found simultaneously. Expressing a relation N and $\Delta\varepsilon'$ obtained from the calibration test under the condition $\Delta\sigma = a$ with $\Delta\sigma$ as a parameter, as found from eq. (7) easily, the curves corresponding to the different values of $\Delta\sigma$ coincide with each other in translating by a distance proportional to the difference between the corresponding values of $\Delta\sigma$, and a value of C_1 in eq. (8) may be found from the distance[3]. The values of C_2 through C_4 may be determined by approximating a combined curve, described to pass through the origin, with eq. (8). The values of C_i should be revised to approximate also the result of calibration test under the condition $\Delta\dot{\sigma} = c$. Judging from the result of calibration test performed, the approximation in the form of eq. (8) has a high accuracy. The values of C_i depend on the wave length of light.

b) Unloading and reversed loading processes In eq. (12a), for a sufficiently low level of $\Delta\sigma(t)$ at the beginning of unloading such that an effect of the third term on the right hand side is not so significant, in a range of $\Delta\bar{\sigma}(t)$ where the first term on the right hand side as well as the second term within square bracket may be negligible, the unloading curve may be approximated by a relation $\Delta\bar{\varepsilon} \simeq \Delta\bar{\sigma}/2G'$. The value of G' may thus be found from the calibration test performed in such a range.

For sufficiently high value of $\Delta\sigma(t)$ at the beginning of unloading such that an effect of the third term on the right hand side of eq. (12a) appears remarkably, in a range of $\Delta\bar{\sigma}(t)$ where the first term on the right hand side as well as the second term within the square bracket are negligibly small, the equation may be expressed by

$$\Delta\bar{\varepsilon}(t) = \frac{\Delta\bar{\sigma}(t)}{2G'} + \frac{B_0' h}{2} e^{b\sqrt{3}(g(t_*))} \sum_{m=0}^{\infty} \frac{(-bh/\sqrt{3})^m}{m!} \left\{ \frac{g(t_*)}{h} \frac{t^{\alpha+m+1} - t_*^{\alpha+m+1}}{\alpha+m+1} - \frac{t^{\alpha+m+2} - t_*^{\alpha+m+2}}{\alpha+m+2} \right\}$$

and

$$g(t_*) = \Delta\sigma(t_*) + ht_*,$$

for a constant rate h of $\Delta\bar{\sigma}(t)$. If the straight line $\Delta\bar{\varepsilon} = \Delta\bar{\sigma}/2G'$ is entered to pass through a point where unloading begins, and if a distance between abscissas of the straight line and the unloading curve is taken in a range where both curves are almost parallel, a value corresponding to the second term of the above relation is obtained. Since the values of α and b have been found from the result in the loading process, the value of B_0' may be determined from the value just found.

When the load is removed suddenly at the beginning of unloading, this corresponds to the conditions $\Delta\bar{\sigma} = d$ (value of $\Delta\sigma$ at the beginning of unloading), $\Delta\sigma = 0$ and $\Delta\dot{\bar{\sigma}} = 0$. Since eq. (5a) becomes as

$$\Delta\dot{\bar{\varepsilon}}(t) = \frac{B_1}{2} \bar{t}^{\beta} d e^{b'd/\sqrt{3}}$$

or

$$\log_{10}(2\Delta\dot{\bar{\varepsilon}}(t)/d) = \log_{10} B_1 + \beta \log_{10} \bar{t} + 0.4343\ b'd/\sqrt{3}, \tag{16}$$

values of B_1, β and b' may be found by the calibration test for more than two different values of d.

With the conditions $\Delta\dot{\bar{\sigma}}(t) = h$ and $\Delta\bar{\sigma}(t) = h\bar{t}$, eq. (12a) is expressed as

$$A_2(t) = \frac{\{\Delta\bar{\sigma}(t)\}^{2n'+1}}{2G'(\sqrt{3}k')^{2n'}}$$

or

$$\log_{10} A_2(t) = (2n'+1)\log_{10}\Delta\bar{\sigma}(t) - \log_{10} 2G'(\sqrt{3}k')^{2n'}, \tag{17}$$

where

$$A_2(t) = \Delta\bar{\varepsilon}(t) - \frac{\Delta\bar{\sigma}(t)}{2G'} - \frac{B_1}{2}\bar{t}^{\beta+1}\Delta\bar{\sigma}(t)\sum_{m=0}^{\infty}\frac{(b'\Delta\bar{\sigma}(t)/\sqrt{3})^m}{m!(\beta+m+2)} + \frac{B_0'h}{2}e^{bg(t*)/\sqrt{3}}$$

$$\times\sum_{m=0}^{\infty}\frac{(-bh/\sqrt{3})^m}{m!}\left[\frac{t^{\alpha+m+2}-t_*^{\alpha+m+2}}{\alpha+m+2} - \frac{g(t_*)}{h}\frac{t^{\alpha+m+1}-t_*^{\alpha+m+1}}{\alpha+m+1}\right]$$

and

$$g(t_*) = ht_* + \Delta\sigma(t_*), \quad B_0' = 0 \quad \text{for} \quad \Delta\sigma(t_*) < |h\bar{t}|.$$

Since the values of $A_2(t)$, $\Delta\bar{\sigma}(t)$ and G' have been obtained, values of n' and k' may be determined by the above relation from the calibration test.

The values of C_5 through C_8 in eq. (9) may be found from the fringe order per unit thickness $\bar{N}(t)$ obtained by the calibration, in the same manner.

4. Evaluation of Fundamental Relations [4]

In the photo-rheologic method, as the time rate of each parameter of each element in a model is considered, a relation between fringe order and time at each element marked by the network incised on each specimen is obtained first from an isochromatic fringe pattern at each instant of deformation of specimen.

As the fringe order may be considered as a function of principal stress difference, a relation between the principal stress difference and time in each element may be obtained. As the location of each element at each instant has been known by the result of test, a distribution of principal stress difference may be obtained by entering the corresponding value of principal stress difference in the location of element at each instant. The relation between the rate of fringe order variation and time may be obtained by finding the gradient on the curve of fringe order versus time, and it corresponds to a relation obtained by differentiating eq. (8) with respect to time,

$$\dot{N}(t) = C_1\Delta\dot{\sigma}(t) + [C_2 + \frac{3}{2}C_3\{\Delta\varepsilon'(t)\}^{1/2} + 2C_4\Delta\varepsilon'(t)]\Delta\dot{\varepsilon}'(t), \tag{18}$$

or by differentiating eq. (9) with respect to time,

$$\dot{\bar{N}}(\bar{t}) = C_5\Delta\dot{\bar{\sigma}}(\bar{t}) + [C_6 + \frac{3}{2}C_7\{\Delta\bar{\varepsilon}(t)\}^{1/2} + 2C_8\Delta\bar{\varepsilon}'(t)]\Delta\dot{\bar{\varepsilon}}'(\bar{t}), \tag{19}$$

where $\Delta\dot{\varepsilon}'(t)$ and $\Delta\varepsilon'(t)$ are obtained by subtracting $\Delta\dot{\sigma}(t)/2G$ and $\Delta\sigma(t)/2G$ from eqs. (4b) and (11b), and $\Delta\dot{\bar{\varepsilon}}(\bar{t})$ and $\Delta\bar{\varepsilon}'(t)$ are obtained by subtracting $\Delta\dot{\bar{\sigma}}(t)/2G'$ and $\Delta\bar{\sigma}(t)/2G'$ from eqs. (5b) and (12b), respectively.

The integral terms in eqs. (11b) and (12b) will be evaluated in detail. Since unknown values $\Delta\sigma(t)$ and $\Delta\bar{\sigma}(t)$ are contained in these integrands, these integrations cannot be performed analytically. Therefore, in the loading process, for example, the corresponding time interval is subdivided into $0\sim t_1$, $t_1\sim t_2$, $\cdots$, $t_n\sim t_{n+1}$, $\cdots$, in which the magnitude of $\Delta\dot{\sigma}(t)$ could be regarded as constant, and the stress at an instant τ in $t_n\sim t_{n+1}$ is approximated as

$$\Delta\sigma(\tau) = \Delta\sigma(t_n) + \Delta\dot{\sigma}(t_n)(\tau - t_n).$$

Then, expressing the integral term in eq. (11b) in the next form

$$\int_0^t \tau^\alpha\Delta\sigma(\tau)e^{(b/2)\Delta\sigma(\tau)}d\tau = \int_0^{t_n}\tau^\alpha\Delta\sigma(\tau)e^{(b/2)\Delta\sigma(\tau)}d\tau + \sum_{m=0}^{\infty}\frac{(b/2)^m}{m!}\int_{t_n}^{t_{n+1}}\tau^\alpha\{\Delta\sigma(\tau)\}^{m+1}d\tau$$

$$+ \int_{t_{n+1}}^{t}\tau^\alpha\Delta\sigma(\tau)e^{(b/2)\Delta\sigma(\tau)}d\tau,$$

the integral of the second term on the right hand side is rewritten as

$$\int_{t_n}^{t_{n+1}} \tau^{\alpha}\{\Delta\sigma(t_n)+\Delta\dot{\sigma}(t_n)(\tau-t_n)\}^{m+1}d\tau.$$

The integral may be evaluated by expanding the integrand into series and integrating by term. As the result, the next relation may be obtained from eq. (11b)

$$\Delta\varepsilon'(t)=\frac{B_0}{2}\Big[\int_0^{t_n}\tau^{\alpha}\Delta\sigma(\tau)e^{(b/2)\Delta\sigma\tau}d\tau+\Delta\dot{\sigma}(t_n)e^{(b/2)p(t_n)}\sum_{m=0}^{\infty}\frac{\{b\Delta\dot{\sigma}(t_n)/2\}^m}{m!}$$

$$\times\Big\{\frac{p(t_n)(t_{n+1}^{\alpha+m+1}-t_n^{\alpha+m+1})}{\Delta\dot{\sigma}(t_n)(\alpha+m+1)}+\frac{t_{n+1}^{\alpha+m+2}-t_n^{\alpha+m+2})}{\alpha+m+2}\Big\}+\int_{t_{n+1}}^{t}\tau^{\alpha}\Delta\sigma(\tau)e^{(b/2)\Delta\sigma\tau}d\tau\Big]$$

$$+\frac{\Delta\sigma(t)}{2G}\Big\{\frac{\Delta\sigma(t)}{2k}\Big\}^{2n}, \tag{20}$$

where

$$p(t_n)=\Delta\sigma(t_n)-\Delta\dot{\sigma}(t_n)t_n.$$

The integration of the third term on the right hand side of eq. (12b) may be performed in almost the same way as before, except that the time is subdivided into $t_*\sim t_1$, $t_1\sim t_2,\cdots$, $t_*\sim t_{n+1},\cdots$. For an integration of the first term on the right hand side of eq. (12b), the next form

$$\Delta\bar{\sigma}(\tau)=\Delta\bar{\sigma}(t_n)+\Delta\dot{\bar{\sigma}}(\bar{t}_n)(\bar{\tau}-\bar{t}_n)$$

may be used for an instant τ in $t_n\sim t_{n+1}$, where $\bar{t}_n=t_n-t_*$. In the same manner, the next relation may be obtained from eq. (12b).

$$\Delta\bar{\varepsilon}'(t)=\frac{B_1}{2}\Big[\int_{t_*}^{t_n}\bar{\tau}^{\beta}\Delta\bar{\sigma}(\tau)e^{(b'/2)\Delta\bar{\sigma}\tau}d\tau+\Delta\dot{\bar{\sigma}}(\bar{t}_n)e^{(b'/2)q(t_n)}\sum_{m=0}^{\infty}\frac{(b'\Delta\dot{\bar{\sigma}}(\bar{t}_n)/2)^m}{m!}$$

$$\times\Big\{\frac{q(t_n)(\bar{t}_{n+1}^{\beta+m+1}-\bar{t}_n^{\beta+m+1}}{\Delta\dot{\bar{\sigma}}(\bar{t}_n)(\beta+m+1)}+\frac{\bar{t}_{n+1}^{\beta+m+2}-\bar{t}_n^{\beta+m+2}}{\beta+m+2}\Big\}+\int_{t_{n+1}}^{t}\bar{\tau}^{\beta}\Delta\bar{\sigma}(\tau)e^{(b'/2)\Delta\bar{\sigma}\tau}d\tau\Big]$$

$$+\frac{\Delta\bar{\sigma}(t)}{2G'}\Big\{\frac{\Delta\bar{\sigma}(t)}{2k'}\Big\}^{2n'}+\frac{B_0'}{2}\Big[\int_{t_*}^{t_n}\tau^{\alpha}\Delta\sigma(\tau)e^{(b/2)\Delta\sigma\tau}d\tau+\Delta\dot{\bar{\sigma}}(\bar{t}_n)e^{(b/2)r(t_n)}$$

$$\times\sum_{m=0}^{\infty}\frac{(-b\Delta\dot{\bar{\sigma}}(\bar{t}_n)/2)^m}{m!}\Big\{\frac{r(t_n)(\bar{t}_{n+1}^{\alpha+m+1}-\bar{t}_n^{\alpha+m+1})}{\Delta\dot{\bar{\sigma}}(\bar{t}_n)(\alpha+m+1)}-\frac{t_{n+1}^{\alpha+m+2}-t_n^{\alpha+m+2}}{\alpha+m+2}\Big\}$$

$$+\int_{t_{n+1}}^{t}\tau^{\alpha}\Delta\sigma(\tau)e^{(b/2)\Delta\sigma\tau}d\tau\Big], \tag{21}$$

where

$$q(t_n)=\Delta\bar{\sigma}(t_n)-\Delta\dot{\bar{\sigma}}(\bar{t}_n)\bar{t}_n \qquad \text{and} \qquad r(t_n)=\Delta\sigma(t_n)+\Delta\dot{\bar{\sigma}}(t_n)t_n.$$

By using these relations, the values of $\Delta\sigma(t_n)$ of each element may be found in each small time interval from the value of $\dot{N}(t)$ or $\dot{\bar{N}}(t)$ of the element obtained by experiment.

4.1 Loading process

If a body is in a natural state in which $\Delta\sigma(t_0)=0$ at $t=t_0=0$, as $\Delta\varepsilon'(t_0)=\Delta\dot{\varepsilon}'(t_0)=0$ may be obtained from eqs. (4b) and (20), a relation $\dot{N}(t_0)=C_1\Delta\dot{\sigma}(t_0)$ is found from eq. (18).

The value of $\Delta\dot{\sigma}(t_0)$ is thus found from the value of $\dot{N}(t_0)$ obtained by experiment, and a value of $\Delta\sigma(t_1)$ may be found by the relation

$$\Delta\sigma(t_1) = \Delta\dot{\sigma}(t_0)(t_1 - t_0).$$

In a period $t_1 \sim t_2$,

$$\Delta\dot{\varepsilon}'(t_1) = \frac{B_0}{2} t_1^{\alpha} \Delta\sigma(t_1) e^{(b/2)\Delta\sigma(t_1)} + \frac{\Delta\dot{\sigma}(t_1)}{2G}(2n+1)\left\{\frac{\Delta\sigma(t_1)}{2k}\right\}^{2n} = E_1 + F_1\Delta\dot{\sigma}(t_1)$$

and

$$\Delta\varepsilon'(t_1) = \frac{B_0}{2}\Delta\dot{\sigma}(t_0)\sum_{m=0}^{\infty}\frac{(b\Delta\dot{\sigma}(t_0)/2)^m}{m!}\frac{t_1^{\alpha+m+2}}{\alpha+m+2} + \frac{\Delta\sigma(t_1)}{2G}\left\{\frac{\Delta\sigma(t_1)}{2k}\right\}^{2n} = G_1$$

are obtained from eqs. (4b) and (20), respectively, where E_1, F_1 and G_1 are known values. Substituting them into eq. (8), the next relation for finding $\Delta\dot{\sigma}(t_1)$ is obtained.

$$\Delta\dot{\sigma}(t_1) = \frac{\dot{N}(t_1) - (C_2 + 3C_3G_1^{1/2}/2 + 2C_4G_1)E_1}{C_1 + (C_2 + 3C_3G_1^{1/2}/2 + 2C_4G_1)F_1}.$$

The value of $\Delta\sigma(t_2)$ is thus found from

$$\Delta\sigma(t_2) = \Delta\sigma(t_1) + \Delta\dot{\sigma}(t_1)(t_2 - t_1).$$

In a period $t_2 \sim t_3$,

$$\Delta\dot{\varepsilon}'(t_2) = \frac{B_0}{2} t_2^{\alpha}\Delta\sigma(t_2) e^{(b/2)\Delta\sigma(t_2)} + (2n+1)\frac{\Delta\dot{\sigma}(t_2)}{2G}\left\{\frac{\Delta\sigma(t_2)}{2k}\right\}^{2n} = E_2 + F_2\Delta\dot{\sigma}(t_2)$$

and

$$\Delta\varepsilon'(t_2) = \frac{B_0}{2}\left[\int_0^{t_1}\tau^{\alpha}\Delta\sigma(\tau)e^{(b/2)\Delta\sigma(\tau)}d\tau + \Delta\dot{\sigma}(t_1)e^{(b/2)p(t_1)}\sum_{m=0}^{\infty}\frac{(b\Delta\dot{\sigma}(t_1)/2)^m}{m!}\right.$$

$$\left.\times\left\{\frac{p(t_1)(t_2^{\alpha+m+1} - t_1^{\alpha+m+1})}{\Delta\dot{\sigma}(t_1)(\alpha+m+1)} + \frac{t_2^{\alpha+m+2} - t_1^{\alpha+m+2}}{\alpha+m+2}\right\}\right] + \frac{\Delta\sigma(t_2)}{2G}\left\{\frac{\Delta\sigma(t_2)}{2k}\right\}^{2n} = G_2$$

are found from eqs. (4b) and (20), respectively, where E_2, F_2 and G_2 are known values. Substituting them into eq. (18), the next relation for finding $\Delta\dot{\sigma}(t_2)$ is obtained.

$$\Delta\dot{\sigma}(t_2) = \frac{\dot{N}(t_2) - (C_2 + 3C_3G_2^{1/2}/2 + 2C_4G_2)E_2}{C_1 + (C_2 + 3C_3G_2^{1/2}/2 + 2C_4G_2)F_2}.$$

The value of $\Delta\sigma(t_3)$ is thus found from

$$\Delta\sigma(t_3) = \Delta\sigma(t_2) + \Delta\dot{\sigma}(t_2)(t_3 - t_2).$$

In the same manner, the value of $\Delta\sigma$ in every instant for each element may be obtained from the corresponding value of $\dot{N}(t)$ obtained by the experiment. When a condition $\Delta\dot{\sigma}(t) < 0$ becomes to hold on the way of calculation, the calculation should be changed to that for unloading process. It is necessary to note that the condition does not always correspond to a condition $\dot{N}(t) < 0$, as easily found from the above relations.

In the next, a case in which $\Delta\sigma(t_0) \neq 0$ at $t = t_0 = 0$ will be discussed. In such a case, as found in eq. (8), fringe order corresponds to the relation

$$N(t_0) = C_1\Delta\sigma(t_0) + C_2\Delta\varepsilon'(t_0) + C_3\{\Delta\varepsilon'(t_0)\}^{3/2} + C_4\{\Delta\varepsilon'(t_0)\}^2, \qquad \text{(a)}$$

and $\Delta\varepsilon'(t_0)$ contained in the relation may be expressed from eq. (20) as follows:

$$\Delta\varepsilon'(t_0) = \frac{\Delta\sigma(t_0)}{2G}\left\{\frac{\Delta\sigma(t_0)}{2k}\right\}^{2n}. \tag{b}$$

The value of $\Delta\sigma(t_0)$ may thus be found by solving a equation obtained by substituting (b) into (a) with the value of $N(t_0)$ obtained by the experiment. Value of $\Delta\varepsilon'(t_0)$ may be found by substituting the value of $\Delta\sigma(t_0)$ into eq. (b). As $\Delta\dot{\varepsilon}'(t_0)$ and $\dot{N}(t_0)$ may be expressed by eqs. (4b) and (18) as

$$\Delta\dot{\varepsilon}'(t_0) = (2n+1)\frac{\Delta\dot{\sigma}(t_0)}{2G}\left\{\frac{\Delta\sigma(t_0)}{2k}\right\}^{2n}$$

and

$$\dot{N}(t_0) = C_1\Delta\dot{\sigma}(t_0) + [C_2+3C_3\{\Delta\varepsilon'(t_0)\}^{1/2}/2 + 2C_4\Delta\varepsilon'(t_0)\}\Delta\dot{\varepsilon}'(t_0),$$

the value of $\Delta\dot{\sigma}(t_0)$ corresponding to $\dot{N}(t_0)$ may be obtained by substituting the values of $\Delta\sigma(t_0)$ and $\Delta\varepsilon'(t_0)$ into them. The procedure after that is the same as before.

4.2 Unloading and reversed loading processes

The evaluation is performed for time intervals $t_* \sim t_1, t_1 \sim t_2, \cdots$ beginning from t_*. At the beginning of unloading, $\Delta\bar{\varepsilon}'(t_*)=0$ is found from eq. (21), and

$$\Delta\dot{\bar{\varepsilon}}'(\bar{t}_*) = -\frac{B_0'}{2}\bar{t}_*^{\alpha}\Delta\sigma(t_*)e^{(b'/2)\Delta\sigma(t_*)} = -H_1$$

is obtained from eq. (5b), where H_1 is a known value. Therefore,

$$\Delta\dot{\bar{\sigma}}(\bar{t}_*) = \{\dot{\bar{N}}(\bar{t}_*) + C_6H_1\}/C_5$$

is obtained from eq. (19), and the values of $\Delta\bar{\sigma}(t_1)$ and $\Delta\sigma(t_1)$ are found from the next relations

$$\Delta\bar{\sigma}(t_1) = \Delta\bar{\sigma}(t_*) + \Delta\dot{\bar{\sigma}}(\bar{t}_*)(t_1 - t_*) = \Delta\dot{\bar{\sigma}}(\bar{t}_*)(t_1 - t_*)$$

and

$$\Delta\sigma(t_1) = \Delta\sigma(t_*) - |\Delta\bar{\sigma}(t_1)|.$$

In a period $t_1 \sim t_2$,

$$\Delta\dot{\bar{\varepsilon}}'(\bar{t}_1) = \frac{B_1}{2}\bar{t}_1^{\beta}\Delta\bar{\sigma}(t_1)e^{(b'/2)\Delta\bar{\sigma}(t_1)} + (2n'+1)\frac{\Delta\dot{\bar{\sigma}}(\bar{t}_1)}{2G'}\left\{\frac{\Delta\bar{\sigma}(t_1)}{2k'}\right\}^{2n'} - \frac{B_0'}{2}\bar{t}_1^{\alpha}\Delta\sigma(t_1)e^{(b'/2)\Delta\sigma(t_1)}$$

$$= K_1 + \Delta\dot{\bar{\sigma}}(\bar{t}_1)L_1 - M_1$$

and

$$\Delta\bar{\varepsilon}'(t_1) = \frac{B_1}{2}\Delta\dot{\bar{\sigma}}(\bar{t}_*)\sum_{m=0}^{\infty}\frac{(b'\Delta\dot{\bar{\sigma}}(\bar{t}_*)/2)^m}{m!}\frac{\bar{t}_1^{\beta+m+2}}{\beta+m+2} + \frac{\Delta\bar{\sigma}(t_1)}{2G'}\left\{\frac{\Delta\bar{\sigma}(t_1)}{2k'}\right\}^{2n'}$$

$$+\frac{B_0'}{2}\Delta\dot{\bar{\sigma}}(\bar{t}_*)e^{(b'/2)\Gamma(t_*)}\sum_{m=0}^{\infty}\left\{\frac{(-b\Delta\dot{\bar{\sigma}}(\bar{t}_*)/2)^m}{m!}\frac{r(t_*)(\bar{t}_1^{\alpha+m+1} - \bar{t}_*^{\alpha+m+1})}{\Delta\dot{\bar{\sigma}}(\bar{t}_*)(\alpha+m+1)}\right.$$

$$\left.-\frac{\bar{t}_1^{\alpha+m+2} - \bar{t}_*^{\alpha+m+2}}{\alpha+m+2}\right\} = P_1,$$

where

$$r(t_*) = \Delta\sigma(t_*) + \Delta\dot{\bar{\sigma}}(\bar{t}_*)t_*,$$

are obtained from eqs. (5b) and (21), respectively, where K_1, L_1, M_1 and P_1 are known values. Therefore,

$$\Delta\dot{\bar{\sigma}}(\bar{t}_1) = \frac{\dot{\bar{N}}(\bar{t}_1) - (C_6 + 3C_7P_1^{1/2}/2 + 2C_8P_1)(K_1 - M_1)}{C_5 + (C_6 + 3C_7P_1^{1/2}/2 + 2C_8P_1)L_1}$$

is obtained from eq. (19), and the values of $\Delta\bar{\sigma}(t_2)$ and $\Delta\sigma(t_2)$ are found from the nex relations,

$$\Delta\bar{\sigma}(t_2) = \Delta\bar{\sigma}(t_1) + \Delta\dot{\bar{\sigma}}(\bar{t}_1)(t_2 - t_1)$$

and

$$\Delta\sigma(t_2) = \Delta\sigma(t_*) - |\Delta\sigma(t_2)|.$$

In a period $t_2 \sim t_3$,

$$\Delta\dot{\bar{\varepsilon}}(\bar{t}_2) = \frac{B_1}{2}\bar{t}_2^{\beta}\Delta\bar{\sigma}(t_2)e^{(b'/2)\Delta\bar{\sigma}(t_2)} + (2n'+1)\frac{\Delta\dot{\bar{\sigma}}(\bar{t}_2)}{2G'}\left\{\frac{\Delta\bar{\sigma}(t_2)}{2k'}\right\}^{2n'} - \frac{B_0}{2}t_2^{\alpha}\Delta\sigma(t_2)e^{(b/2)\Delta\sigma(t_2)}$$

$$= K_2 + \Delta\dot{\bar{\sigma}}(\bar{t}_2)L_2 - M_2$$

and

$$\Delta\dot{\bar{\varepsilon}}(t_2) = \frac{B_1}{2}\left[\int_{t_*}^{t_1}\bar{\tau}^{\beta}\Delta\bar{\sigma}(\tau)e^{(b'/2)\Delta\bar{\sigma}(\tau)}\,d\tau + \Delta\dot{\bar{\sigma}}(\bar{t}_1)e^{(b'/2)q(t_1)}\sum_{m=0}^{\infty}\frac{(b'\Delta\dot{\bar{\sigma}}(\bar{t}_1)/2)^m}{m!}\right.$$

$$\times\left\{\frac{q(t_1)(\bar{t}_2^{\beta+m+1} - \bar{t}_1^{\beta+m+1})}{\Delta\dot{\bar{\sigma}}(\bar{t}_1)(\beta+m+1)} + \frac{\bar{t}_2^{\beta+m+2} - \bar{t}_1^{\beta+m+2}}{\beta+m+2}\right\}\Big] + \frac{\Delta\bar{\sigma}(t_2)}{2G'}\left\{\frac{\Delta\bar{\sigma}(t_2)}{2k'}\right\}^{2n'}$$

$$+\frac{B_0'}{2}\left[\int_{t_*}^{t_1}\tau^{\alpha}\Delta\sigma(\tau)e^{(b/2)\Delta\sigma(\tau)}\,d\tau + \Delta\dot{\bar{\sigma}}(\bar{t}_1)e^{(b/2)r(t_1)}\sum_{m=0}^{\infty}\frac{(-b\Delta\dot{\bar{\sigma}}(\bar{t}_1)/2)^m}{m!}\right.$$

$$\times\left\{\frac{r(t_1)(t_2^{\alpha+m+1} - t_1^{\alpha+m+1})}{\Delta\dot{\bar{\sigma}}(\bar{t}_1)(\alpha+m+1)} - \frac{t_2^{\alpha+m+2} - t_1^{\alpha+m+2}}{\alpha+m+2}\right\}\Big] = P_2$$

are obtained from eqs. (5a) and (21), respectively, where K_2, L_2, M_2 and P_2 are known values. Therefore,

$$\Delta\dot{\bar{\sigma}}(\bar{t}_2) = \frac{\dot{\bar{N}}(\bar{t}_2) - (C_6 + 3C_7P_2^{1/2}/2 + 2C_8P_2)(K_2 - M_2)}{C_5 + (C_6 + 3C_7P_2^{1/2}/2 + 2C_8P_2)L_2}$$

is obtained from eq. (19), and the values of $\Delta\bar{\sigma}(t_3)$ and $\Delta\sigma(t_3)$ may be found by the next relations,

$$\Delta\bar{\sigma}(t_3) = \Delta\bar{\sigma}(t_2) + \Delta\dot{\bar{\sigma}}(\bar{t}_2)(t_3 - t_2)$$

and

$$\Delta\sigma(t_3) = \Delta\tau(t_*) - |\Delta\bar{\sigma}(t_3)|.$$

In the same manner, the value of $\Delta\sigma(t)$ at every instant in the unloading and reversed loading processes may be obtained for each element. When a condition $\Delta\dot{\bar{\sigma}}(\bar{t}) < 0$ becomes to hold on the way of calculation, the element enters into a reloading process, and this process

corresponds to unloading and reversed loading processes against the preceding unloading. Then, by taking an instant of the beginning of reloading t_{**} as an origin, almost the same relations as those used between the loading and unloading processes may be used between the unloading and reloading.

5. Separation of Principal Stresses

By means of the above mentioned procedure, a distribution of principal stress difference within model specimen may be found at every instant. When the isoclinic parameter indicates the direction of principal stress, stress components may be found by using the shear-difference method. However, it cannot be said theoretically that the isoclinic parameter in the viscoplastic deformation indicates always the direction of principal stress, because the optical anisotropy depends on the viscoplastic strain besides the elastic one as mentioned above.

If the principal axis of stress does not rotate in a element during deformation, since the principal axis of each kind of strain does not rotate, it may be said that the isoclinic parameter indicates the direction of principal stress. On the other hand, for a stress trajectory with a corner of right angle for example, as in the case when the torsion is applied to a thin-walled cylindrical celluloid specimen after its plastic deformation under tension, it has been ascertained that the isoclinic parameter may indicate within a tolerable error the direction of principal stress after rotation of principal axis of stress even for a fairly large value of pre-strain[5),6)]. The stress trajectory with corner corresponds to the most severe case whereas the trajectory of each element appearing in most plastic work may be considered as that of so-called "trajectory of small curvature"[7)]. Therefore, it may be said that any significant error cannot arise by considering that the isoclinic parameter indicates the direction of principal stress in such case.

6. Effect of Principal Stress Ratio

As mentioned above, the characteristic values in eqs. (4) through (6) depend on the principal stress ratio. However, the ratio cannot be obtained before finding stress distribution, and thus the effect of principal stress ratio cannot be used directly on finding stress distribution. The following procedure may be performed in this respect.

i) Characteristic values are found first by calibration test for each value of principal stress ratio. As the result, a relation between characteristic values and principal stress ratio is obtained, where the ratio of axial stress σ_1 to oil pressure σ_2 has $\sigma_1/\sigma_2=\infty$ for axial stress only and $\sigma_1/\sigma_2=0$ for pressure only, and other values between them correspond to every other case.

ii) Judging from the deformation state of specimen, a value of σ_1/σ_2 near to its average is assumed. A stress distribution is obtained for every instant by using the characteristic values corresponding to the assigned principal stress ratio. The result may be regarded as a first approximation of this analysis.

iii) Since the distribution of principal stress ratio may be found from the result obtained above, a principal stress ratio at every instant is found for each element. Then, each characteristic value for each element may be determined by the result of calibration test as a function of time.

iv) Repeating the analysis by using the characteristic values thus obtained, a stress distribution may be found by taking account of the effect of principal stress ratio. Since the use of characteristic value as a function of time is complicated while the effect of principal stress ratio is not so significant for stress state, some approximate methods may be applied to simplify the calculation.

7. Similarity Conditions and Possibility of Similar Model Test[8)]

In order that the above mentioned method acquires the utility as a practical method of

experimental stress analysis, however, it must be able to determine quantitatively actual processes of inelatic deformation of prototype from the results of the corresponding model test. It is thus necessary to derive conditions for the process in model test to be similar to the actual one in prototype, and to ascertain a possibility of performing similar model test to an assigned prototype.

When the prototype includes not only inelastic material but also elastic one, as in the case of plastic work, the similarity must be specified as regards a system of these materials. However, if the combination of elastic and inelastic materials is chosen so that the ratio of elastic modulus of the former to one of representative material constants of the latter in model is equal to that in prototype, and if the process of deformation in the inelastic material of model is similar to that of the prototype, similarity condition of a two-dimensional elastic body which occupies a simply connected region is satisfied automatically. Thus, as regards the similarity of inelastic material which contacts with elastic one, the similarity should be discussed only with respect to inelastic material.

In general process of non-steady inelastic deformation, strain state of an element at a given instant cannot be specified only by the stress state at the instant because it depends on the preceding history of strain. Strain state in such a material should thus be related to the current stress as well as to the preceding strain. Accordingly, the stress and strain rates of each element in prototype and the corresponding model must be provided by the kinematic and dynamic equations expressed in terms of these rates in addition to a proper constitutive equation.

To describe such processes accurately with reference to elements prescribed at initial state, relations based on the theory of finite deformation should be assumed because the above mentioned method deals with large deformation generally. However, the finite deformation theory is too complicated to establish fundamental relations in model test including a consideration of similarity conditions. In the above mentioned method, an analysis is thus carried out in pursuit of each element, by calculating an increment of each variable with reference to a given instant according to relations expressed with respect to principal axes, and integrating these increments with respect to time to obtain the stress and strain at each instant. Relations governing such increments can be formulated by the theory of infinitesimal deformation. Then, the similarity conditions in the infinitesimal deformation are examined.

Fundamental relations in the infinitesimal deformation take the following forms, where the cartesian coordinates (x_i) are used and partial derivatives with respect to time t and coordinates x_i are denoted by $\dot{(\ )}$ and $(\ )_{,i}$, respectively:

1) spin tensor

$$\Omega_{ij} = (v_{j,i} - v_{i,j})/2 \tag{22}$$

2) strain rate tensor

$$\dot{\varepsilon}_{ij} = (v_{i,j} + v_{i,j})/2, \tag{23}$$

3) equation of motion

$$\dot{\sigma}_{ij} + \dot{X}_i = \rho \ddot{v}_i, \tag{24}$$

4) equation of compatibility

$$\dot{\varepsilon}_{ij,kl} + \dot{\varepsilon}_{kl,ij} - \dot{\varepsilon}_{ik,jl} - \dot{\varepsilon}_{jl,ik} = 0, \tag{25}$$

5) constitutive equations

$$\dot{e}_{ij} = \frac{1}{2G}\dot{s}_{ij} + \frac{2n+1}{4G}\left(\frac{J_2}{k^2}\right)^n \frac{\dot{J}_2}{J_2} s_{ij} + \frac{1}{2} B_0 t^{\alpha} e^{b\sqrt{J_2}} s_{ij}, \tag{26a}$$

$$\dot{\varepsilon}_{ll} = \frac{1-2\nu}{2G(1+\nu)} \dot{\sigma}_{mm}, \tag{26b}$$

6) boundary conditions

$$v_i = V_i \qquad \text{on } S_u, \tag{27a}$$

$$\dot{\sigma}_{ij}\nu_j = \dot{T}_i^{\nu} \qquad \text{on } S_\sigma, \tag{27b}$$

7) initial conditions

$$u_i = u_{i0} \qquad \text{in } R, \quad \text{on } S, \tag{28a}$$

$$\sigma_{ij} = \sigma_{ij0} \qquad \text{in } R, \quad \text{on } S. \tag{28b}$$

The above relations involve twenty-four physical quantities. Since the characteristic length of the system is also taken into account, the number of total physical quantities specifying the process of deformation is $n = 25$.

7.1 Dimensionless expressions and similarity conditions

According to the π-theorem of dimension analysis, the number of independent dimensionless quantities m in a physical phenomenon consisting of n physical quantities is given by $m = n - r$, where r is the maximum number of physical quantities which cannot make any dimensionless quantity by any combination of them.

On the other hand, conditions for a designed model to be similar to a prescribed prototype may be divided into the conditions concerning the geometry, the boundary and initial conditions and those of mechanical properties of materials. The former conditions among them can be satisfied by properly determining experimental conditions such as shape and size of model specimen, load and displacement acting to it and their rates and so on. Body force may be usually neglected in comparison with external load. As the inertia term in the equation of motion can be neglected usually, the similarity regarding density is not necessary to be considered. Thus, the most important conditions in realizing similar model test are those concerning the mechanical properties of materials. It is thus necessary to carry out the calibration test with materials of prototype and model to ascertain the similarity between them before model test.

The similarity conditions regarding mechanical property of material generally consist of six relations in the constitutive equations (26). It is thus difficult to find a material and an experimental condition such that all of these conditions can be satisfied precisely for any range of stress and strain. In order to discuss the similarity of material property, a relevant range of stress or strain is thus specified for convenience in a scheduled model test. In the following, as two representative examples of the range of strain encountered in the above mentioned method, a case of relatively small strain which corresponds to structural analysis and that of large strain corresponding to plastic work are selected, and fundamental relations are rewritten by the corresponding dimensionless quantities to discuss the similarity conditions in these cases.

7.2 Dimensionless expressions and similarity conditions in model test of structural analysis

In the analysis of structural elements, ranges of strain occuring in prototype and model may be comparable with the maximum elastic strain, because the plastic region is usually constrained by surrounding elastic regions. To discuss the similarity of stress-strain relation in this range, it is thus convenient to use a characteristic length ℓ, the elastic modulus G and a

reference quantity $(2GB_0)^{-1/(1+\alpha)}$ for obtaining dimensionless quantities. In this case, however, one can reduce the number of independent dimensionless quantities m by one less than the number $(n-r)$ given by the π-theorem of dimension analysis, by applying a dimensionless scale-factor $\varepsilon_0 = k/2G$ to strain, displacement and their rates. Twenty-one independent dimensionless quantities are thus defined as follows:

$$\sigma_{ij}^* = \sigma_{ij}/k, \quad s_{ij}^* = s_{ij}/k, \quad \sigma_{ij0}^* = \sigma_{ij0}/k, \quad J_2^* = J_2/k^2, \quad T_i^{\nu *} = T_i^{\nu}/k,$$
$$X_i^* = \ell X_i/k, \quad \varepsilon_{ij}^* = 2G\varepsilon_{ij}/k, \quad e_{ij}^* = 2Ge_{ij}/k, \quad u_i^* = 2Gu_i/k\ell,$$
$$u_{i0}^* = 2Gu_{i0}/k, \quad v_i^* = 2G(2GB_0)^{-1/(1+\alpha)}v_i/k\ell, \quad V_i^* = 2G(2GB_0)^{-1/(1+\alpha)}V_i/k\ell,$$
$$\Omega_{ij}^* = 2G(2GB_0)^{-1/(1+\alpha)}\Omega_{ij}/k, \quad x_i^* = x_i/\ell, \quad t^* = (2GB_0)^{1/(1+\alpha)}t, \quad \nu_j^* = \nu_j,$$
$$n^* = n, \quad \alpha^* = \alpha, \quad b^* = kb, \quad \nu^* = \nu, \quad \rho^* = \ell^2(2GB_0)^{2/(1+\alpha)}\rho/2G \tag{29}$$

The fundamental relations (22) through (28) lead to the equivalent dimensionless forms by rewriting them by means of these dimensionless quantities. Then, necessary and sufficient conditions for a model test of structural analyses to be similar to a prototype are, besides the condition of geometric similarity, written as

$$(\sigma_{ij0}/k)_p = (\sigma_{ij0}/k)_m, \quad (T_i^{\nu}/k)_p = (T_i^{\nu}/k)_m, \quad (\ell X_i/k)_p = (\ell X_i/k)_m,$$
$$(2Gu_{i0}/k\ell)_p = (2Gu_{i0}/k\ell)_m, \quad \{2G(2GB_0)^{-1/(1+\alpha)}V_i/k\ell\}_p = \{2G(2GB_0)^{-1/(1+\alpha)}V_i/k\ell\}_m,$$
$$(\nu_j)_p = (\nu_j)_m \tag{30a}$$

for the boundary and initial conditions, and

$$(n)_p = (n)_m, \quad (\alpha)_p = (\alpha)_m, \quad (kb)_p = (kb)_m, \quad (\nu)_p = (\nu)_m,$$
$$\{\ell^2(2GB_0)^{2/(1+\alpha)}\rho/2G\}_p = \{\ell^2(2GB_0)^{2/(1+\alpha)}\rho/2G\}_m \tag{30b}$$

for the material constants. The indices p and m correspond with prototype and model, respectively. When these conditions are satisfied, the state of deformation in prototype can be determined by the following relations:

$$(\sigma_{ij}/k)_p = (\sigma_{ij}/k)_m, \quad (2G\varepsilon_{ij}/k)_p = (2G\varepsilon_{ij}/k)_m, \quad (x_i/\ell)_p = (x_i/\ell)_m,$$
$$\{(2GB_0)^{1/(1+\alpha)}t\}_p = \{(2GB_0)^{1/(1+\alpha)}t\}_m. \tag{30c}$$

7.3 Dimensionless expressions and similarity conditions in model test of plastic work

In the case of plastic work, a relevant range of strain is sufficiently large in comparison with elastic strain. As found in the later experiment, for the total strain of softened celluloid equal to that of mild steel, the ratio of elastic strain to the total strain in celluloid is far larger than that in mild steel. Hence, as it is impossible to expect the similarity between stress-strain diagrams of both materials to hold accurately in the entire range of strain, we discuss the similarity with special emphasis on a range of large strain. Then, it is reasonable to take k and (kB_0) together with a characteristic length ℓ to obtain dimensionless quantities. Since the number of total physical quantities and that of independent dimensionless quantities are $n = 25$ and $r = 3$ in this case, the following $m = n - r = 22$ independent dimensionless quantities are obtained.

$$\sigma_{ij}^* = \sigma_{ij}/k, \quad s_{ij}^* = s_{ij}/k, \quad \sigma_{ij0}^* = \sigma_{ij0}/k, \quad J_2^* = J_2/k^2, \quad T_i^{\nu *} = T_i^{\nu}/k,$$
$$X_i^* = \ell X_i/k, \quad \varepsilon_{ij}^* = \varepsilon_{ij}, \quad e_{ij}^* = e_{ij}, \quad u_i^* = u_i/\ell, \quad v_i^* = (kB_0)^{-1/(1+\alpha)}v_i/\ell,$$

$$V_i^*=(kB_0)^{-1/1+\alpha}V_i/\ell,\quad \Omega_{ij}^*=(kB_0)^{1/1+\alpha}\Omega_{ij},\quad x_i^*=x_i=x_i/\ell,\quad t^*=(kB_0)^{1/1+\alpha}t,$$
$$\nu_j^*=\nu_j,\quad G^*=2G/k,\quad n^*=n,\quad \alpha^*=\alpha,\quad b^*=kb,\quad \nu^*=\nu,$$
$$\rho^*=\ell^2\rho(kB_0)^{2/1+\alpha}/k,\quad u_{i0}^*=u_{i0}/\ell. \tag{31}$$

The fundamental equations (22) through (28) again lead to the equivalent ones by using dimensionless quantities. Then, necessary and sufficient conditions for similarity, besides the conditions of geometric similarity, are expressed as

$$(\sigma_{ij0}/k)_p=(\sigma_{ij0}/k)_m,\quad (T_i^\nu/k)_p=(T_i^\nu/k)_m,\quad (\ell X_i/k)_p=(\ell X_i/k)_m,$$
$$(u_{i0}/\ell)_p=(u_{i0}/\ell)_m,\quad \{(kB_0)^{-1/1+\alpha}V_i/\ell\}_p=\{(kB_0)^{-1/1+\alpha}V_i/\ell\}_m,\quad (\nu_j)_p=(\nu_j)_m. \tag{32a}$$

for the boundary and initial conditions, and

$$(2G/k)_p=(2G/k)_m,\quad (n)_p=(n)_m,\quad (\alpha)_p=(\alpha)_m,\quad (kb)_p=(kb)_m,$$
$$(\nu)_p=(\nu)_m,\quad \{\ell^2(kB_0)^{2/1+\alpha}\rho/k\}_p=\{\ell^2(kB_0)^{1/1+\alpha}\rho/k\}_m. \tag{32b}$$

for material constants. When these conditions are satisfied, the state of deformation of prototype is determined by the following relations:

$$(\sigma_{ij}/k)_p=(\sigma_{ij}/k)_m,\quad (\varepsilon_{ij})_p=(\varepsilon_{ij})_m,\quad (x_i/\ell)_p=(x_i/\ell)_m,$$
$$\{(kB_0)^{1/1+\alpha}t\}_p=\{(kB_0)^{1/1+\alpha}t\}_m. \tag{32c}$$

7.4 Experimental examination of similarity condition on the characteristic values

To analyse actual processes of deformation in a prototype by model test, we must find first suitable materials and conditions of model test so that the mechanical property of model materials under such conditions may be similar to that of prototype under working conditions over a relevant range of strain. Now, we examine experimentally a mechanical similarity between mild steel S15C as prototype and solftened celluloid as model as regards two kinds of model test described in the preceding section, and discuss a possibility of realizing similar model test.

For the examination of mechanical similarity of prototype and model-material, one must only ascertain that stress-strain relations of both materials are described accurately by the constitutive equations (26) and the similarity condition (30b) or (32b) holds for their material constants. Since it is difficult to verify these relations for arbitrary stress history and arbitrary stress state, we examine them by a uniaxial tensile test at constant rate of stress. In the following discussion, true stress and logarithmic strain are assumed. Because the effect of volumetric strain (26b) is relatively small, Poisson's ratio is assumed to be $\nu=1/2$ for both materials, which warrants a part of the similarity condition (30b) or (32b). Then, the constitutive equation (26) lead to the following form in the case of uniaxial tension

$$\dot{\varepsilon}=\frac{1}{3G}\left\{1+(2n+1)\left(\frac{\sigma}{\sqrt{3}k}\right)^{2n}\right\}\dot{\sigma}+\frac{1}{3}B_0t^\alpha e^{b/\sqrt{3}\sigma}\sigma, \tag{33}$$

where σ and ε denote the stress and strain, respectively. For constant rate of stress $\dot{\sigma}=c$, and with an initial condition $\sigma=0$ at $t=0$, the relation (33) can be integrated to yield

$$\varepsilon=\frac{ct}{3G}\left\{1+\left(\frac{ct}{\sqrt{3}k}\right)^{2n}\right\}+\frac{1}{3}B_0c\int_0^t\tau^\alpha e^{b/\sqrt{3}c\tau}d\tau. \tag{34}$$

Now, it is necessary to perform calibration test under uniaxial tension at given rates of stress and determine the material constants so that resulting stress-strain relations may be described accurately by the relation (34). For uniaxial tension at constant rate of stress, elastic and plastic strains represented by the first term of the relation (34) are uniquely determined by the stress at that instant, while a viscous strain corresponding to the second term of the relation

depends not only on stress but also history of stress and hence on the stress rate. Consequently, for determining material constants concerning viscous strain, calibration test must be performed several times at different rates of stress. The calibration test is performed for mild steel of 0.15 percent carbon steel S15C at 450 and 500°C, and the results of calibration test for cellulo id performed at 55.5°C are used.

For the calibration test of mild steel, the stress rates are assumed as $\dot{\sigma}$ = 50, 10, 2 and 0.4 kg/mm²/hr for each temperature, and the maximum stress is assumed to be 40 kg/mm². An accuracy of loading and that of strain measurement were better than 0.02 kg/mm² and 2×10^{-5}, respectively. To reduce the error due to scattering of experimental results, four tests are repeated for each case.

a) Experimental result for mild steel

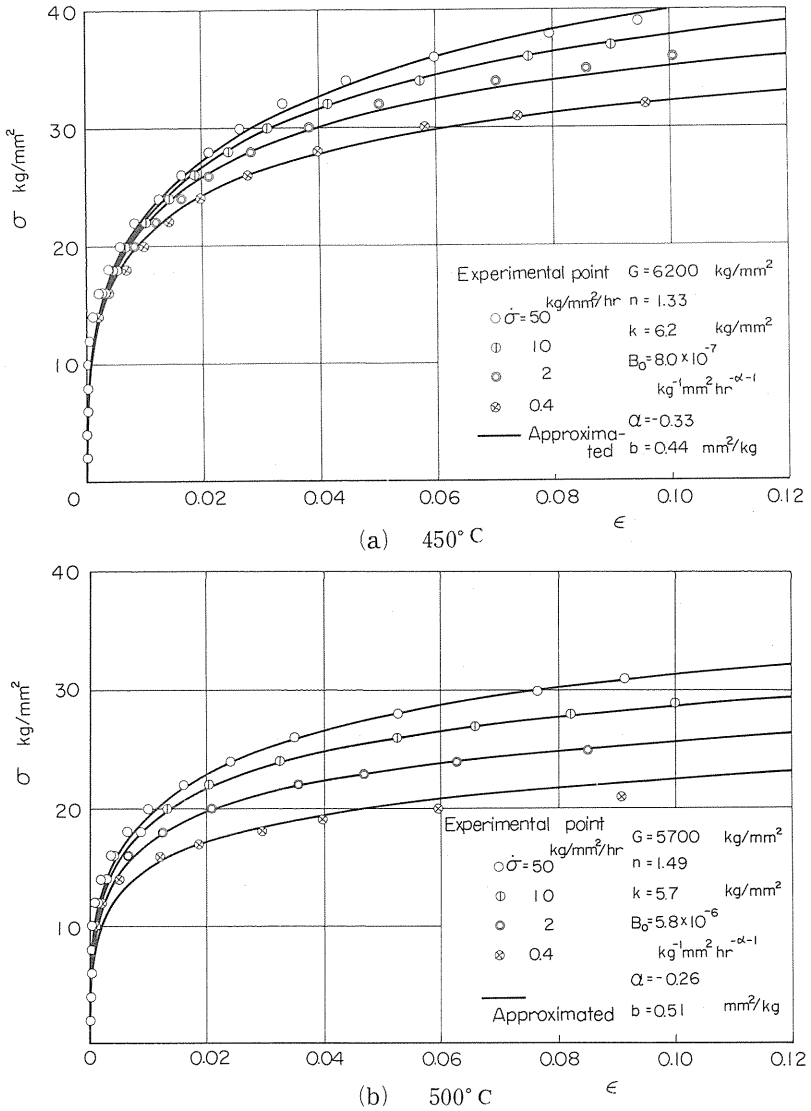

Fig. 2 Stress-strain relation of mild steel, (a) 450°C, (b) 500°C

Results of experiment at 450 and 500°C are shown with the small circles in Fig. 2. The scattering of the results obtained by four tests was less than 2 percent, and the circles in the figure represent average values of them. The solid curves in Fig. 2 were obtained by approximating the experimental result with eq. (34), and the corresponding material constants are shown in the figure. As found in the figure, eq. (34) describes the experimental results fairly well.

b) Experimental results for celluloid

Small circles in Fig. 3 show the experimental results of celluloid at 55.5°C obtained by uniaxial tension at constant stress rates[2], and all of them are average values obtained by each two specimens. The solid curves in the figure are results of application of eq. (34) to the experimental results, and the corresponding material constants are shown in the figure. Except some results in the range of $\varepsilon = 0.01 \sim 0.03$, the solid curves represent well the experimental results.

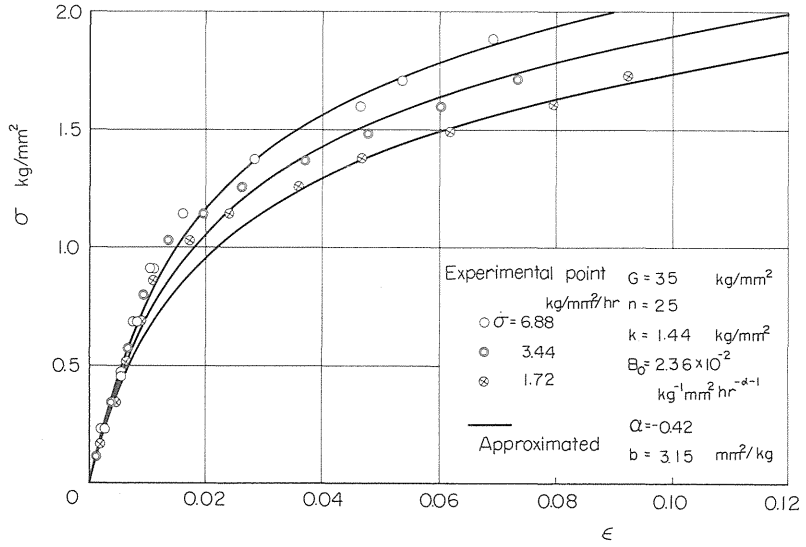

Fig. 3 Stress-strain relation of celluloid (55.5°C)

7.5 Discussion of similarity conditions according to the experimental results

a) Model test for structural analysis

Relevant ranges of strain in structural analysis are usually several times of maximum elastic strain. Because the experimental results for steel have been obtained over sufficiently wide range of strain (Fig. 2), a necessary range may be taken up from it.

Figure 4 is obtained by enlarging a range of small strain in Fig. 2 and the solid curves show results of application of eq. (34) to the experimental results with emphasis on this range of strain. Equation (34) represents the experimental results within errors of 4 and 8 percent for the case of 450 and 500°C, respectively.

Now, let's examine the mechanical similarity in the present case between celluloid and steel. A direct method for this is to compare the material constants of celluloid shown in Fig. 3 with those of steel in Fig. 4 with respect to the conditions (30b) derived before. Dimensionless quantities specified by the relation (30b) for these materials and difference between them are shown in Table 1. As found in the table, relative difference between these dimensionless quantities is about 5 percent, and coincide fairly well with each other. Nevertheless, in the case of steel at 450°C, the values of α and kb are a little different from those of

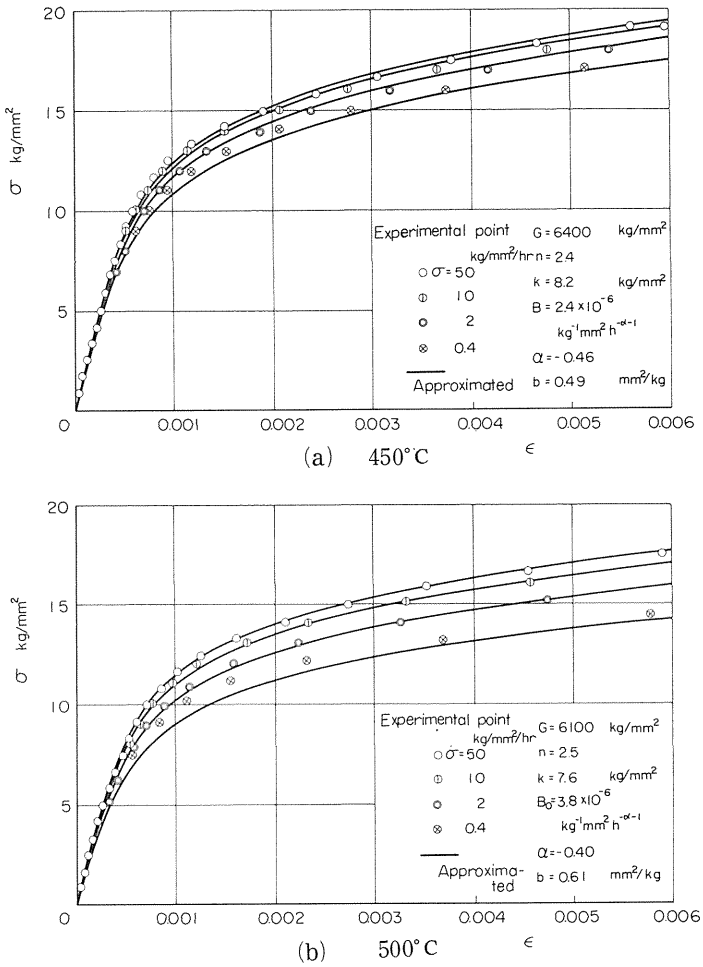

Fig. 4 Stress-strain relation of mild steel (with emphasis on the range of small strain), (a) 450°C, (b) 500°C

celluloid, and hence the accuracy of similarity of the stress-strain relation of steel to that of celluloid is supposed to decrease for larger values of time and stress. However, the effect of the difference found in Table 1 on the actual properties of materials can be clarified only by a quantitative examination.

Table 1 Comparison between dimensionless material constants of prototype and model (model test of structural analysis)

Dimensionless material constants	A Celluloid	B Steel (450°C)	$\frac{A-B}{B_1}\times 100$ (%)	B_2 Steel (500°C)	$\frac{A-B_2}{B_2}\times 100$ (%)
n	2.5	2.4	4.2	2.5	0.0
α	− 0.42	− 0.46	− 8.7	− 4.0	5.0
kb	4.54	4.02	12.9	4.64	− 2.2
ν	0.5	0.5	0.0	0.5	0.0

Figure 5 shows a comparison between the dimensionless stress-strain relations of steel and those of celluloid. The solid curves in the figure are plotted by reducing the curves in Fig. 4 by means of the corresponding material constants and for the corresponding rate of stress, while the dashed curves are dimensionless stress-strain curves of celluloid calculated by using the material constants shown in Fig. 3 for the same values of dimensionless rate of stress as those of steel. As shown in Fig. 5, the dimensionless stress-strain relation of celluloid coincides with those of steel at 450 and 500°C within errors of 5 and 8 percent, respectively.

It has been ascertained that the softened celluloid at 55.5°C may be a similar model material to mild steel S15C at 450 and 500°C with sufficient accuracy. Therefore, for the processes of non-steady inelastic deformation of structural elements consisting of such mild steel, a similar model test can be performed by using such celluloid as a model material and by selecting the test conditions properly so that the boundary and the initial condition may satisfy the condition (30a).

The deformation state of prototype can thus be determined from the results of model test together with the relation (30c).

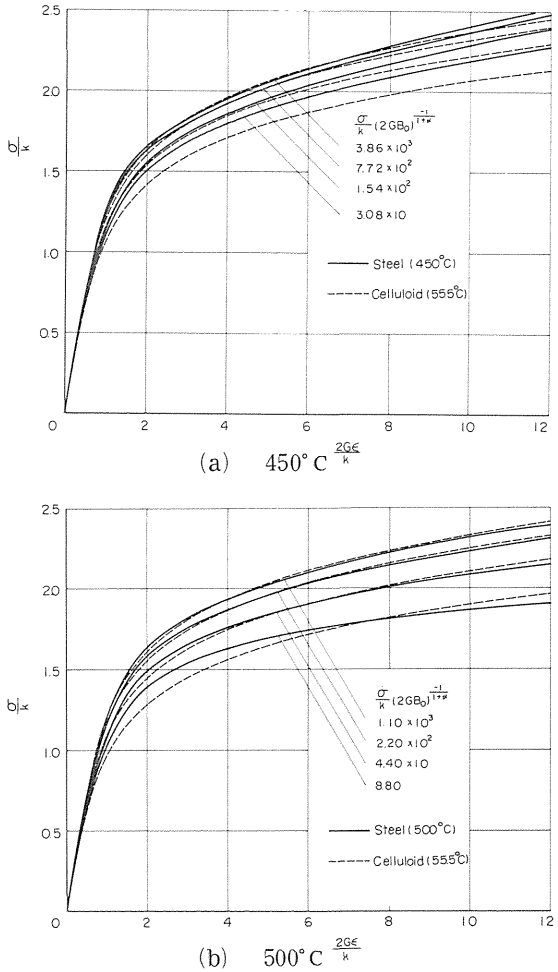

Fig. 5 Comparison between dimensionless stress-strain relations of mild steel and celluloid (model test of structural analysis) (a) 450°C, (b) 500°C

b) Model test for plastic work

Similar results for a model test of plastic work are shown in Figs. 6 through 8. Though the similarity condition between the prototype- and the model-material are given by the relation (32b), it is generally difficult to find a test condition under which these six relations are satisfied for whole range of stress or strain. Figures 6 and 7 are thus plotted by applying eq. (34) again to the experimental results in Figs. 2 and 3 with special emphasis on the range of large strain. Except a range of small strain, eq. (34) describes the experimental results within an error of 10 percent. In the range of large strain where the present problem is concerned mainly, an agreement of the solid curves with the experimental results is especially good.

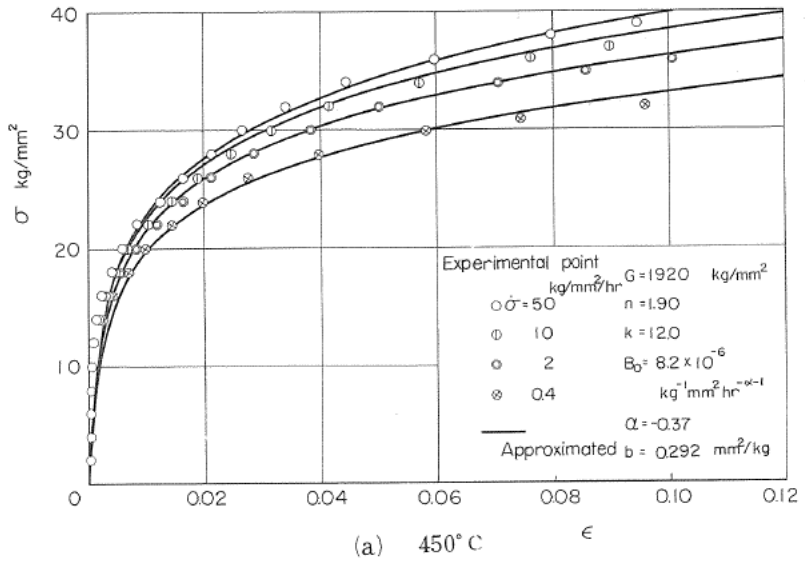

(a) 450°C

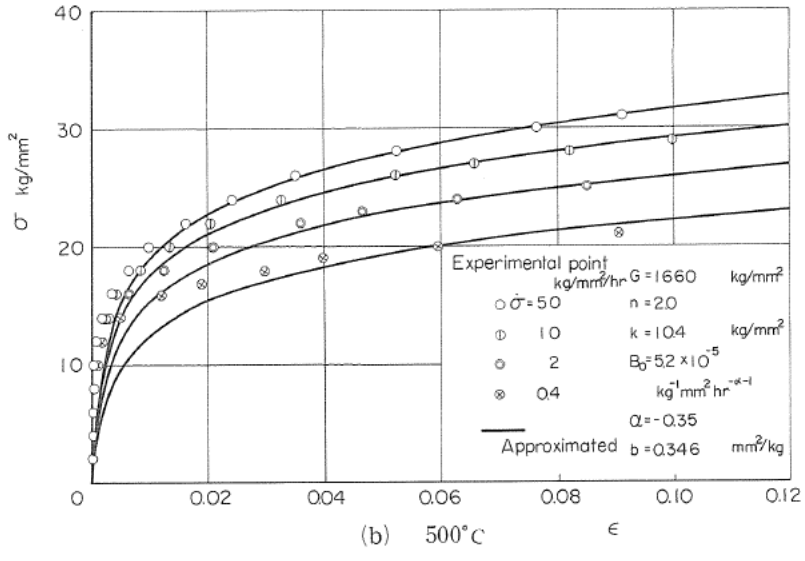

(b) 500°C

Fig. 6 Stress-strain relation of mild steel (with emphasis on the range of large strain) (a) 450°C, (b) 500°C

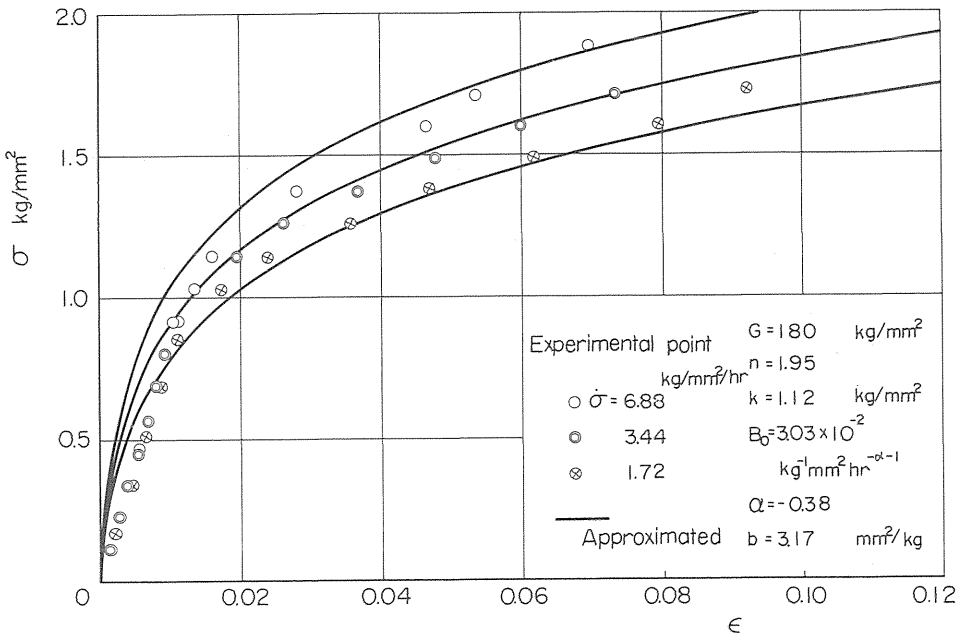

Fig. 7 Stress-strain relation of celluloid (with emphasis on the range of large strain)

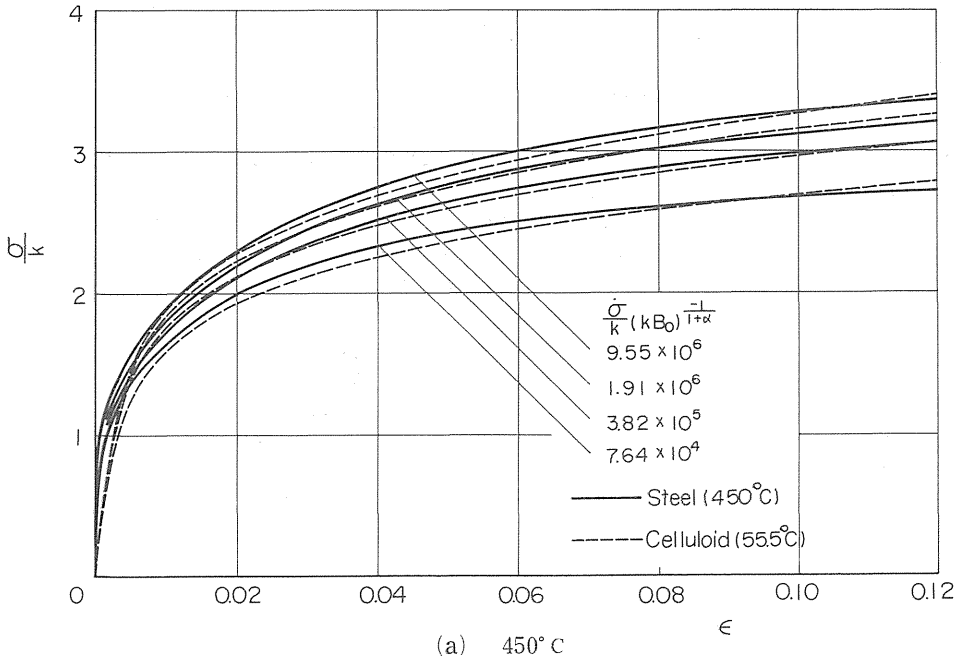

Fig. 8 Comparison between dimensionless stress-strain relations of mild steel and celluloid (model test of plastic works)

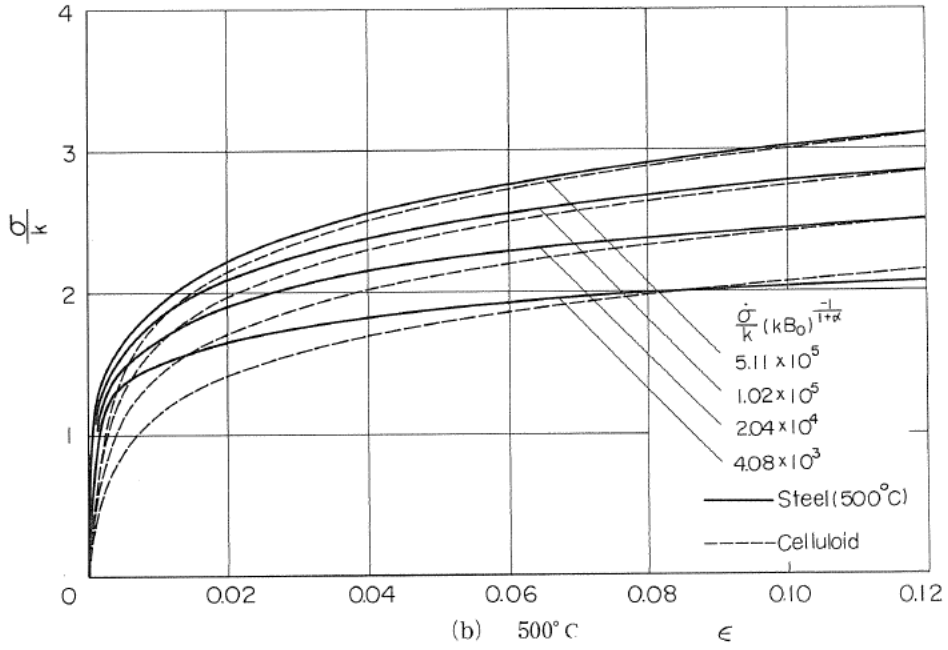

Fig. 8 Comparison between dimensionless stress-strain relations of mild steel and celluloid (model test of plastic works)

Table 2 shows a comparison of the dimensionless material constants calculated from the values in Figs. 6 and 7. It will be noticed that the similarity condition (32b) is satisfied within an error of several percent in every case.

Finally, the dimensionless stress-strain relations calculated from the material constants in Figs. 6 and 7 are plotted in Fig. 8. The solid and dashed curves in this figure indicate relations obtained by rewriting the stress-strain curves of steel in Fig. 6 and those calculated by the material constants of celluloid in Fig. 7 for the same values of dimensionless stress rates as those of steel, respectively. As found in the figure, the agreement of solid and dashed curves is satisfactory except in the range of small strain of the steel at 500°C, and the mechanical similarity between these materials holds well especially in the range of large strain. Accordingly, for the experimental analysis of plastic work of mild steel at 450 and 500°C by means of photo-rheologic method, a similar model test may be performed by using the softened celluloid at 55.5°C examined here as the model material.

Table 2 Comparison between dimensionless material constants of prototype and model (model test of plastic work)

Dimensionless material constants	A Celluloid	B_1 Steel (450°C)	$\frac{A-B_1}{B_1}\times 100$ (%)	B_2 Steel (500°C)	$\frac{A-B_2}{B_2}\times 100$ (%)
$2G/k$	323	320	0.9	319	1.3
n	1.95	1.90	2.6	2.00	− 2.5
α	− 0.38	− 0.37	− 2.7	− 0.35	− 8.6
kb	3.55	3.50	1.4	3.60	− 1.4
ν	0.5	0.5	0.0	0.5	0.0

Part II Applications for Model Tests of Plastic Work

1. Introduction

Some applications of the above mentioned method are described to show its availability for the model test of plastic works. In general plastic works, the plastic deformation of work-piece is very large and an effect of viscosity appears in real materials which leads to a re-distribution of stress during deformation, and the conventional photoplasticity is thus unsuitable to analyse the stress state in work-piece. The photo-rheology may thus be said to be only one method for analysing the stress state within such bodies. In model tests of plastic works using this method, Araldite in a glassy elastic state and a softened celluloid at a suitable temperature are used as model materials of tool and work-piece, respectively. Since the stress state within tools may be found together with that within work-piece subjected to plastic work by using photoelasticity and photo-rheology, the stress states and their time dependence on the contact surfaces of tool and work-piece also may be found easily. This is an excellent merit of this method which enables us to investigate minutely an exquisite behavior of materials around the contact surface.

2. Strip Drawing Through Roller-Dies[9]

As the first example, a model test of strip drawing through roller-dies may be mentioned. At a suitable temperature, a softened celluloid strip as work-piece was drawn plastically through a gap between freely rotating disks of Araldite in a glassy elastic state. The photo-rheology together with the photoelasticity was applied for analysing the stress states within the strip and roller-dies as well as on their contact surfaces. The accuracy of photo-rheology was verified to be comparable with that of photoelasticity, by comparing the distribution of normal stress component on the contact surface of strip obtained by photo-rheology with that of roller-dies obtained by photoelasticity and referring the condition of continuity of normal stresses on both sides of that surface.

2.1 Experimental apparatus

Figure 9 shows an apparatus used. In the figure, a celluloid strip is drawn upwards by a static load through a gap between Aradite roller-dies. The celluloid strip is restricted by a pair of thick glass plates on both surfaces, in order to prevent any change in thickness and thus ensuring a state of plane strain during drawing. To minimize frictional resistance on the contact surfaces between the strip and the glass plates, the glass plates pressed against the strip are supported by ball bearings on their back surfaces so that the plates may move vertically with the strip. The apparatus is kept in an oil bath filled with spindle oil heated at 65° C. Since the deformation behavior of celluloid at that temperature is sensitive to temperature, its variation and non-uniformity must be kept as small as possible. Therefore, in the present experiment, a thirmister-thermometer of minimum scale 0.05° C is used to regulate and measure

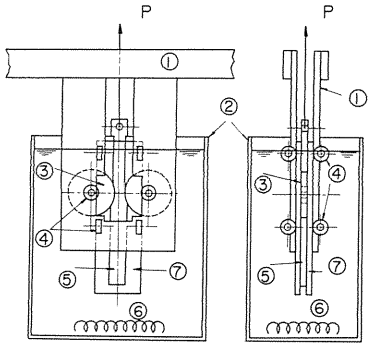

① Supporting Frame ⑤ Test piece of strip
② Oil Bath ⑥ Heater
③ Test piece of Roller dies ⑦ Glass plate
④ Ball bearing

Fig. 9 Experimental apparatus

the temperature, and the variation and non-uniformity of temperature around the specimen are kept within ± 0.05°C.

2.2 Test specimen

The shapes and sizes of specimens are shown in Fig. 10. The reduction ratios selected are r = 10, 15.5, 20 and 25 percent. The strip specimen is covered with a square grid of 1 mm distance to measure the strain state during deformation, and the die specimen is covered with a bunch of radial lines to measure the relative displacement of the work-piece on their contact surface.

From the result of a calibration test using two Araldite specimens at the testing temperature 65° C, it has been ascertained that Araldite was kept in a perfectly glassy elastic state with E = 234 kg/mm² and fringe stress 0.162 kg/mm² per unit thickness.

Calibration test for the softened celluloid at 65°C has been performed by using a combined loading of oil pressure and uniaxial tension. The characteristic values obtained from the calibration test for $\sigma_1/\sigma_2 = -1$ at the testing temperature 65°C are shown in Table 3.

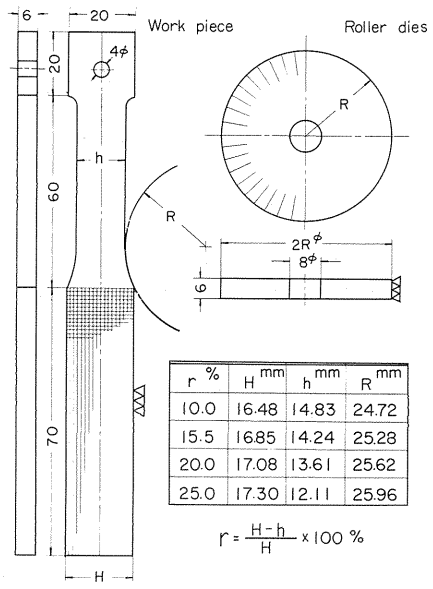

r %	H mm	h mm	R mm
10.0	16.48	14.83	24.72
15.5	16.85	14.24	25.28
20.0	17.08	13.61	25.62
25.0	17.30	12.11	25.96

$r = \frac{H-h}{H} \times 100\ \%$

Fig. 10 Shapes and sizes of specimens

Table 3 Characteristic values of softened celluloid heated at 65°C ($\sigma_1/\sigma_2 = -1$)

B_0	α	b	$2G$	$\sqrt{3}k$	n	$2G'$	B_1	β
1.80×10^{-4}	−0.274	6.78	39.8	0.967	2.03	148	1.20×10	−0.490

B'_0	b'	C_1	C_2	C_3	C_4	C_5	C_6
0.27×10^{-4}	5.98	0.21	1.5	0.30	0.10	0.16	1.4

2.3 Experimental procedure

The experiment is performed for the reduction-ratio $r = (H-h)/H$ shown in Fig. 10, and the ratio of the roller radius R to the width of strip H is 1.5. The drawing load P is selected so that the flowing speed of the strip at the entry to the dies is 0.2 mm/min for each experiment corresponding to the above mentioned values of r. Since both the roller and the strip are kept in the oil bath, the contact surface are considered to be sufficiently well lubricated.

The isochromatic and isoclinic fringes are recorded photo-graphically together with the deformed grid. The former is taken through a monochromatic filter of λ = 546.1 nm, and the latter is recorded without filter in separating the former with the use of a colour film at a slight over-exposure. A photograph of the deformed grid for obtaining the strain state of the strip also is taken without a polariscope.

2.4 Results of experiment

Figure 11 shows an isochromatic fringe photograph for r = 15.5 percent taken in a dark field, and an example of isoclinic fringe photograph (r = 15.5 percent, isoclinic parameter 0°) is shown in Fig. 12. Out of the isochromatic and isoclinic fringe patterns obtained for each value of r, those for r = 15.5 percent are shown in Figs. 13(a) and (b).

The drawing load were obtained as P = 9.75, 18.68, 28.70 and 39.60 kg for r = 10, 15.5, 20 and 25 percent, respectively.

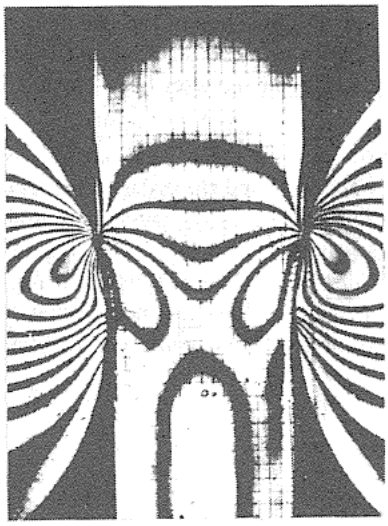

Fig. 11 Isochromatic fringe photograph (r = 15.5 percent, dark field)

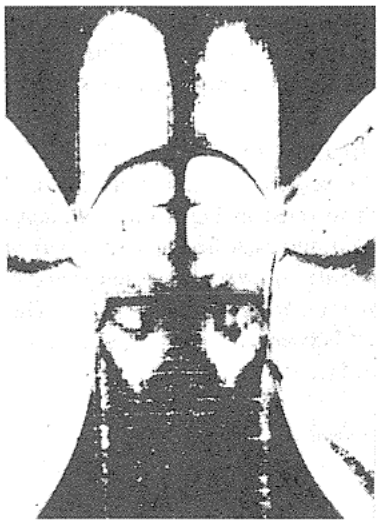

Fig. 12 Isoclinic fringe photograph (r = 15.5 percent, 0°)

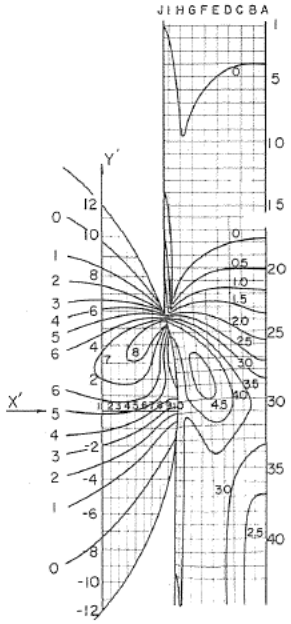

Fig. 13(a) Isochromatic fringe pattern (r = 15.5 percent)

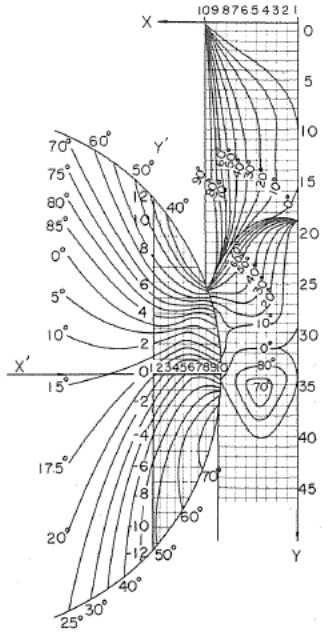

Fig. 13(b) Isoclinic fringe pattern (r = 15.5 percent)

2.5 Principal stress and strain differences in the strip

Some of the characteristic values are affected by the principal stress ratio σ_1/σ_2, and it is necessary to improve the accuracy of the analysis by using the characteristic values involved by considering the effect of σ_1/σ_2. The value of σ_1/σ_2 must, however, be different at every point in the strip, and, moreover, these values are unknown before the analysis is made. Thus, as an approximation, distributions of the principal stresses σ_1 and σ_2 were obtained by using the proposed method with the corresponding values of Table 3. In the analysis for obtaining the principal stress differences depending on the fringe order N, the fundamental equations may be evaluated by the method mentioned in Chapter 4 of Part I by using a digital computer for any element of strip along its flow line; the latter is found as a longitudinal line of the grid deformed during the flow of the strip. The shear-difference method was used for finding the stress components from the principal stress difference and the isoclinic parameter found by the experiment.

Distributions of the value of σ_1/σ_2 along some flow lines in the roll-gap are shown in Fig. 14. In the figure, letters indicating the location of the flow-line and the order of the section correspond to those in Fig. 13(a). As shown in Fig. 14, the value of σ_1/σ_2 undergoes considerable change along each flow-line in a part where the strip is subjected to plastic drawing. Thus the mean values of σ_1/σ_2 for each element along its flow-line in the interval shown in Fig. 14 is used for the corresponding analysis. The dashed lines in Fig. 14 show the mean values, and the relation between the mean values of σ_1/σ_2 and the corresponding elements herein obtained is shown in Fig. 15.

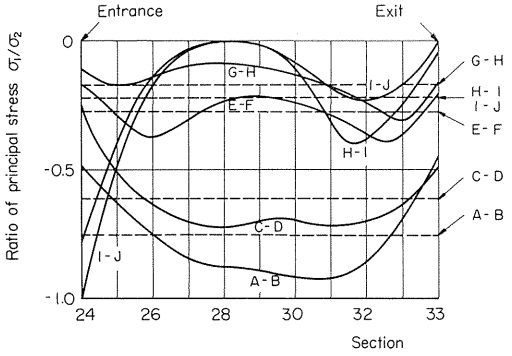

Fig. 14 Distributions of the value of σ_1/σ_2

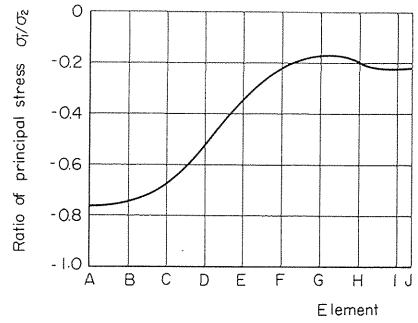

Fig. 15 Relation between the mean value of σ_1/σ_2 and location of the element

Relying on Fig. 15, calibration tests for the strip were performed with $\sigma_1/\sigma_2 = -0.76$, -0.65, -0.35 and 0, and the relation between $\Delta\sigma$ and $\Delta\varepsilon$ obtained from the calibration test is shown in Fig. 16. The relation between the characteristic values and the values of σ_1/σ_2 obtained from the result of test shown in Fig. 16 are shown in Fig. 17. The values of C_1 through C_6 are not affected by the value of σ_1/σ_2. Because the values of G', B_1, β, B_0' and b' are also not so seriously affected by the value of σ_1/σ_2 owing to the fact that these values correspond to the unloading strain $\Delta\bar{\varepsilon}$, which is less than the loading strain $\Delta\varepsilon$, it may be considered that the effect of σ_1/σ_2 on the value of G', B_1, β, B_0' and b' is negligible.

By using the characteristic values herein obtained, the above mentioned calculation was repeated to find the principal stress difference taken into account the effect of principal stress ratio of each element along each flow-line for each value of r. For obtaining a distribution of the principal stress difference in the strip, the value of principal stress difference at each instant

thus obtained was entered on the corresponding location of the element along the flow-line. Distributions of the principal stress difference in the strip thus obtained for r = 15.5 percent, as an example, are shown in Fig. 18, where x and y coordinates are designated as those in Fig. 13(b) independent of the notation A, B, ··· , J and 1, 2, ··· in Fig. 13(a) expressing the deformed grid in the strip.

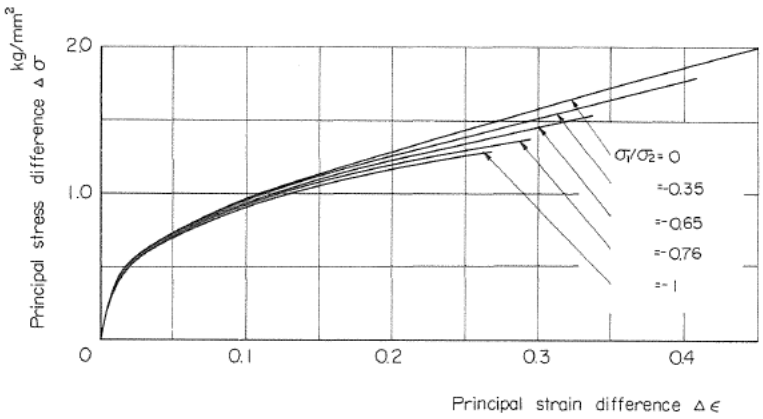

Fig. 16 Relation between $\Delta\sigma$ and $\Delta\varepsilon$ obtained by calibration test

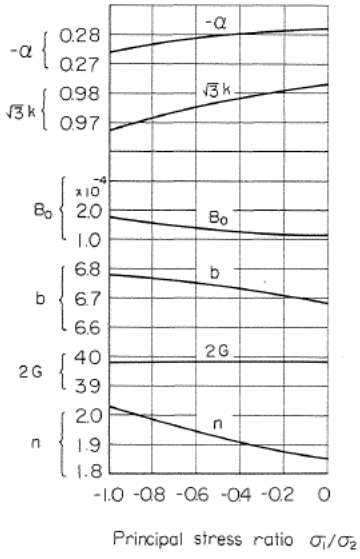

Fig. 17 Relation between characteristic value and σ_1/σ_2

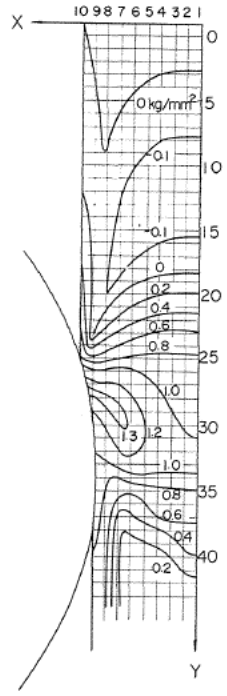

Fig. 18 Distributions of the principal stress differences (r = 15.5 percent)

The principal strain difference and the direction of the principal strain may be found from the following relations depending on accurately measured values obtained from the photograph of the deformed grid by using a magnifying projector:

$$\Delta\varepsilon = \ln \frac{\left[\frac{(1+\varepsilon_x)^2+(1+\varepsilon_y)^2}{2} + \sqrt{\left\{\frac{(1+\varepsilon_x)^2-(1+\varepsilon_y)^2}{2}\right\}^2 + (1+\varepsilon_x)^2(1+\varepsilon_y)^2\cos^2\lambda}\right]}{(1+\varepsilon_x)(1+\varepsilon_y)\sin\lambda} \tag{35}$$

and

$$\tan 2\psi = \frac{2(1+\varepsilon_x)(1+\varepsilon_y)\cos\lambda}{(1+\varepsilon_x)^2-(1+\varepsilon_y)^2} \tag{36}$$

ψ is an acute angle between the direction of the principal strain and the tangential direction to the flow-line of the considered element at the corresponding point, and λ denotes an angle between two lines of the grid after deformation, which were perpendicular to each other at first. Figure 19 shows, as an example, the relations between the values of $\Delta\varepsilon$ and ψ thus obtained and the location of element (section number in Fig. 13(a)) in the case of r = 15.5 percent. Solid and chain curves show the values of ψ and $\Delta\varepsilon$ obtained by eqs. (35) and (36). In the figure, the maximum strain rate about 0.005/min occuring in the element (I-J) and between the sections 22 and 23 corresponds to about a half of the strain rate used for the calibration test. For comparison, the value of $\Delta\varepsilon$ obtained by eq. (11b) or eq. (12b) is described by the dashed lines. The values of $\Delta\varepsilon$ obtained by eq. (11b) or eq. (12b) is less by a few percent than that obtained by eq. (35). This seems to arise from errors in applying the relation (11b) or (12b) derived under the assumption that the direction of principal strain always coincides with the tangential direction to the flow-line of the element and the assumption to formulate the properties of model material. As shown in the figure, the above mentioned derivation does not differ so much for each value of ψ. Thus the error in formulating the material properties may be said to be more significant than those arising the assumption on the direction of principal strain.

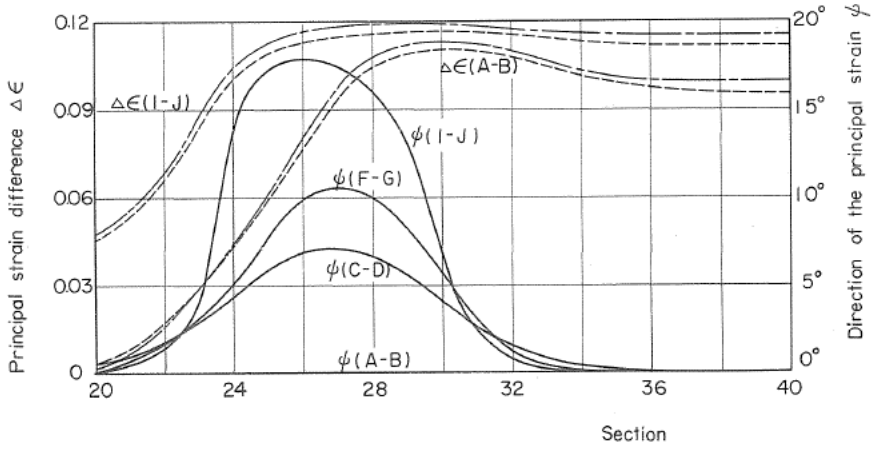

Fig. 19 Relation between $\Delta\varepsilon$ or ψ and the location of element on each flow-line (r = 15.5 percent)

2.6 Stress distributions within roller-dies and strip

Stress analysis within roller dies was performed by using the shear-difference method together with the isochromatic and isoclinic fringe patterns obtained by the experiment. As the method cannot be applied directly to sections passing through contact surface, a section crossing

with free surface should be selected as a base section. Thus a section having a distance $x' = 0.775R$ (R denotes roller radius) from the center of the roller (Fig. 13 (a) and (b)) was selected. The interval between $0.775R$ and R of x' was divided equally into 9 parts of $0.025R$, and sections dividing these parts were designated as the sections 1, 2, ··· , 10. In the y'-direction, sections having a distance $0.05R$ were designated as the sections −12, −11, ··· , 0, ··· , 12. As an example of the results obtained, distributions of stress components on the sections $y' = 0$, 3 and 6 are shown in Fig. 20. In the figure, the values of σ_x and σ_y on the contact surface (dashed line) were obtained by extrapolation from the values of stress components and their derivatives at the nearest meshed points.

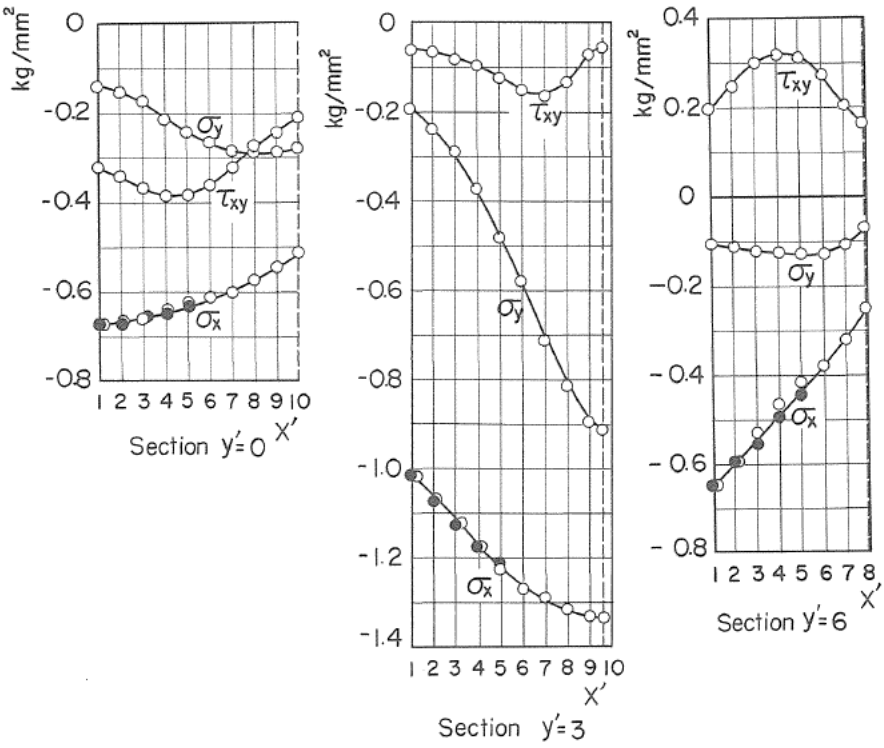

Fig. 20 Distribution of stress components within roller-dies (r = 15.5 percent)

For the stress analysis of the strip which is flowing plastically, the shear-difference method may be applied together with the distribution of principal stress difference shown in Fig. 18 and the isoclinic pattern shown in Fig. 13(b). Because of the symmetry, only one side of the strip with respect to its center should be considered. Designation of each section parallel to the x- and y-directions is shown in Fig. 13(b) and 18, where the sections $x = 1, 2, \cdots 10$ divide the half-width of the strip equally, and the sections $y = 1, 2, \cdots$ divide the strip in the same interval in the y-direction.

For the reason mentioned above, stress components were analysed first in the x-direction along the section $y = 10$. By using the result herein obtained as boundary values, the analyses were performed in the y-direction along the sections $x = 1, 2, \cdots, 10$. The analyses also may be performed independently on each section parallel to the x-direction, starting from their free boundary before the section makes contact with the dies. Some examples of the analysis are

shown in Figs. 21(a) through (d), in the case of r = 15.5 percent and on the sections y = 18, 25, 30 and 44. In these figures, the open and solid circles show the results obtained by the former analysis and the value of σ_y obtained by the latter analysis, respectively. As shown in these figures, the corresponding values of σ_y agree well with each other. The values of σ_x and σ_y on the contact surface were obtained by the same method as in the case of roller-dies. The value of shear stress τ_{xy} was found directly from the experimental result. The maximum shear stress $\tau_{max} = (\sigma_1 - \sigma_2)/2$ and the mean stress $\bar{\sigma} = (\sigma_x + \sigma_y)/2$ are entered on the assumption that the state is of plane strain and that there is no volumetric strain.

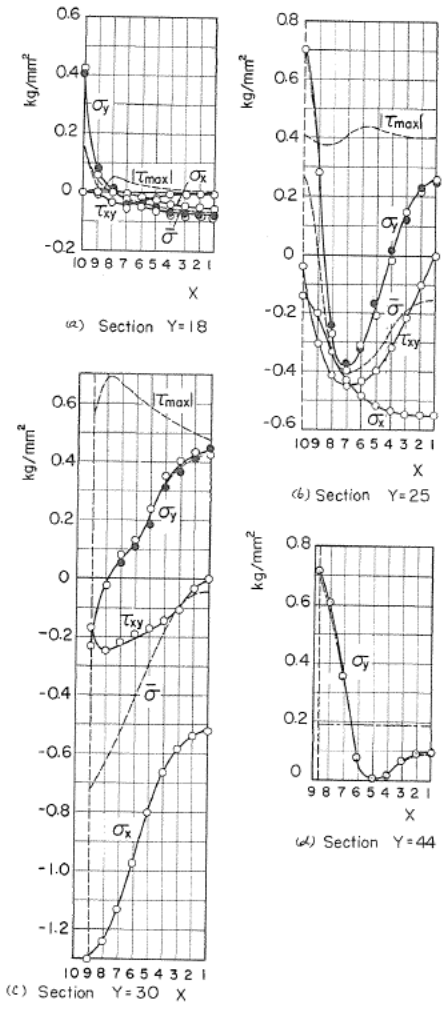

Fig. 21 Distribution of stress components within the strip (r = 15.5 percent)

2.7 Stress distribution on the contact surface

The distributions of contact pressure and frictional shear stress on the contact surface of strip and roller are shown in Figs. 22 through 25 in relation to ϕ indicating the angle between the normal to the contact surface and the y'-direction. In these figures, the solid and dashed curves describe the results on the strip-side obtained by photo-rheology and that on the roller-side

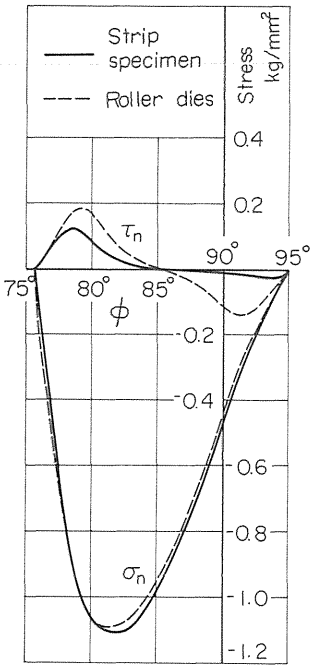

Fig. 22 Distribution of normal pressure σ_n and frictional shear stress τ_n on the contact surface (r = 10 percent)

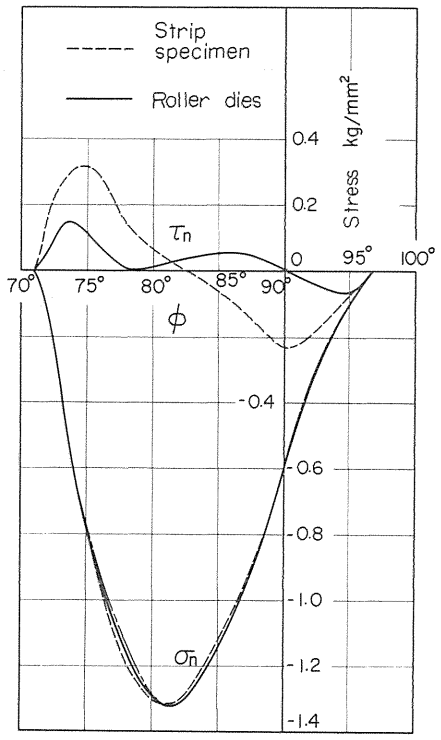

Fig. 23 Distributions of normal pressure σ_n and frictional shear stress τ_n on the contact surface (r = 15.5 percent)

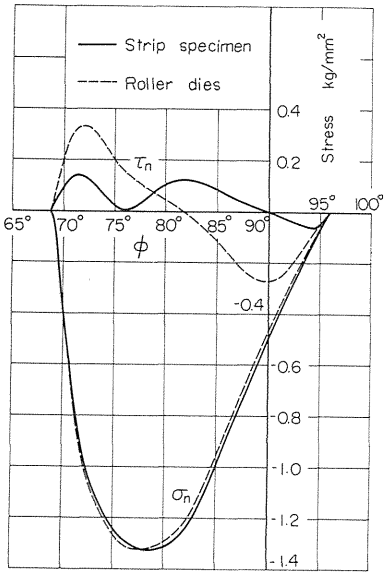

Fig. 24 Distributions of normal pressure σ_n and frictional shear stress τ_n on the contact surface (r = 20 percent)

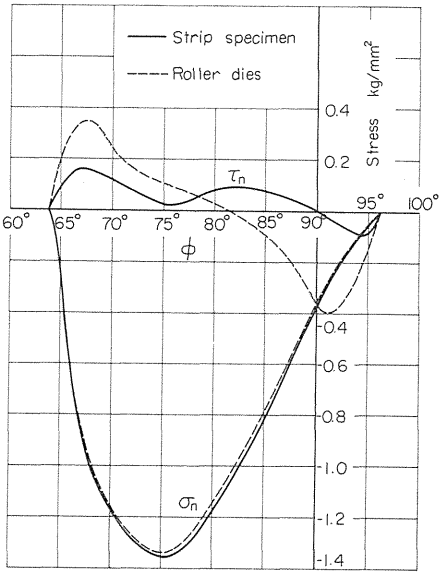

Fig. 25 Distributions of normal pressure σ_n and frictional shear stress τ_n on the contact surface (r = 25 percent)

obtained by photoelasticity. As shown in these figures, both values of σ_n obtained independently on both sides agree with each other almost completely. On the roller-side, values of frictional force acting in opposite directions on the contact surface agree with each other with little error for each value of r.

2.8 Discussion and conclusion

In the above analyses using the shear-difference method, two values of the components σ_y obtained independently along the different paths agree well with each other. This confirms the accuracy of the results as found by the numerical integration.

In the strip, the sum of σ_y on every cross section across the contact surface should be equal to the difference between the drawing load and the sum of the components in the y-direction of σ_n and τ_n acting on the contact surface subsequent to that section. Denoting the former and the latter as A and B, respectively, the disparity between A and B was examined on some cross sections.

Table 4 Comparison of A and B

Section	27	29	31	33	35
A (kg)	6.7	12.7	17.2	19.0	19.0
B (kg)	6.4	12.0	16.6	19.2	19.5
$\frac{A-B}{B} \times 100$ (%)	4.8	5.6	3.5	−1.0	−2.6

An example of these results is shown in Table 4 for $r = 15.5$ percent. In the table, the errors are less than a few percent. Moreover, before or after the contact surface, the sum of σ_y on every cross section should be equal to zero or the drawing load P. In the results of these analyses, this condition is satisfied for each value of r. This ensures that the effect of friction on the contact surfaces between the strip and the glass plates is not significant.

The equality of contact pressures on the contact surface, obtained independently from both sides of the roller and the strip, ensures that the condition of continuity for the normal stress components on the contact surface is fulfilled.

Thus the suitability and accuracy of the photo-rheology, together with the meaning to be attributed to the isoclinic parameter appearing in the plastically deformed body, are proved for the model test of plastic work.

Distributions of the frictional shear stress τ_n on the contact surfaces of the roller and the strip differ significantly from each other. This seems to be due to the fact that the strip is flowing plastically so the speed of each element of the strip may vary with location, while the roller rotates as an elastic body being affected by the viscous flow of the lubricant squeezed toward both sides of a point where the contact pressure has its maximum value. Thus the difference between the value of τ_n on each surface may be roughly estimated by assuming a steady lubrication at each of the parallel walls; Fig. 26 shows the supposed situation at the strip and roller at any point on the contact surface. In the figure, U and h denote a relative speed of the strip to the roller and the thickness of lubricant. If the lubricant is assumed to flow only in the x-direction with a velocity u, the Navier-Stokes equation without compressibility will be $\partial\sigma_n/\partial x = \mu\nabla^2 u$, where μ is a coefficient of viscosity, and σ_n will be

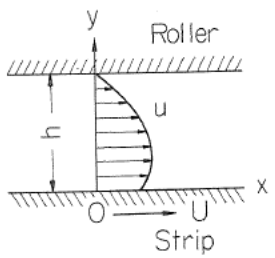

Fig. 26 Scheme of a flow of lubricant

independent of y. From the condition of continuity $\partial u/\partial x = 0$, u becomes a function of y only, and the above equation becomes as $d\sigma_n/dx = \mu(d^2u/dy^2)$. Considering the boundary values, the solution of the equation is found as

$$u = (1-y/h)U - \{y(h-y)/2\mu\}(d\sigma_n/dx).$$

Thus the shear stress on the roller surface and the strip surface will be

$$\tau_{n1} = (\tau_{xy})_{y=h} = -\mu U/h + (h/2)(d\sigma_n/dx)$$

and

$$\tau_{n2} = (\tau_{xy})_{y=0} = -\mu U/h - (h/2)(d\sigma_n/dx),$$

and the difference between them will be

$$\bar{\tau}_n = \tau_{n1} - \tau_{n2} = h(d\sigma_n/dx).$$

The value $\bar{\tau}_n$ will be the above-mentioned difference.

By the results of the above estimation, at a point of the maximum value of σ_n, the value of τ_{n_1} should be equal to that of τ_{n_2}. This requirement is satisfied completely in Figs. 23 and 24 and with slight errors in Figs. 22 and 25.

In the strip at a sufficient distance after leaving the dies, as shown in Fig. 21(d), the distribution of σ_y is not uniform over the section though the stress state should be of uniaxial tension, judging from the corresponding isoclinic pattern. Because the mean value of σ_y becomes zero when the drawing load is released, the distribution of residual stress may be found as the difference between the value σ_y and its mean value shown in Fig. 21(d) with the chain line.

For improving the accuracy of results, in the above analysis, the characteristic values taking account of the effect of σ_1/σ_2 were used. In order to examine the extent of improvement, in the case of r = 15.5 percent, the improved result was compared with that using the values of Table 3 only obtained as a first approximation. The latter value is entered as the chain curve in Figs. 21 and 23. As shown in these figures, the difference between them is very small. It may thus be said that the above-mentioned improvement taking account of the effect of σ_1/σ_2 and containing a lengthy calculation is not really necessary.

3. Effect of Back Tension on the Strip Drawing Through Roller-Dies [10]

The back tension method has been considered in the wire-drawing in which a backward tension is applied to a part of blank before drawing while the blank is drawn by a drawing load through dies, and the merits of this method are mentioned to be a reduction of die-resistance and the corresponding reduction of drawing power and drawing temperature as well as a raise of yield point of manufactures. These merits have been found from actual operations or experiments relying on actual experiences, and thus have not yet been analysed by relating the variation of stress states within blank and dies due to back tension, mainly because any suitable analysis method have been unable to measure the stress states.

However, such measurements are easily performed by using photo-rheology together with the softened celluloid and Araldite as model materials of strip and roller-dies.

3.1 Experimental apparatus

Figure 27 shows an apparatus used in which a device to apply back tension P_2 is supplemented to the one used in the above-mentioned experiment. The back tension P_2 is applied in the same direction as the drawing load P_1 through a piano-wire and ball bearings as shown in Fig. 27.

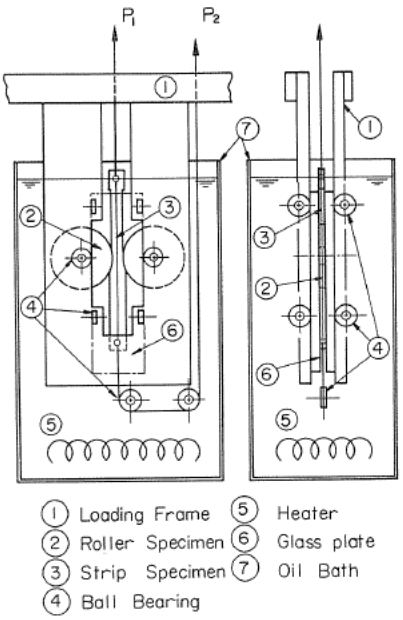

Fig. 27 Experimental apparatus

3.2 Specimens

a) Roller-Dies Roller specimen is a disk finished from Araldite plate of 6 mm thick without initial stress and whose shape and size are shown in Fig. 28. Reduction-ratio of strip width r = 15.5 percent and R/H = 1.5 are selected, where R and H denote the radius of roller-die and the strip width before drawing. Araldite is kept in a perfectly glassy elastic state and has values of fringe stress 0.161 kg/mm² per unit thickness and Young's modulus E = 234 kg/mm².

b) Strip The strip specimen is finished from a transparent celluloid plate of 6 mm thick as shown in Fig. 28 and a square grid is incised for identifying each element.

The characteristic values of the celluloid are the same as mentioned in the preceding experiment.

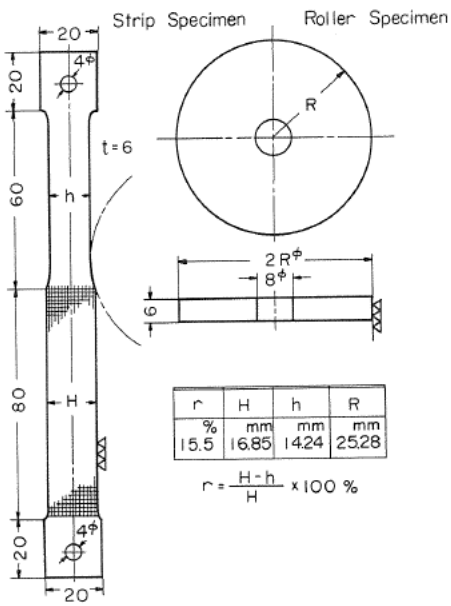

Fig. 28 Shapes and sizes of specimens

3.3 Experimental procedure

The experiment is performed for P_2/P_1 = 0, 1/4, 1/3 and 1/2 in the case of r = 15.5 percent and R/H = 1.5. The drawing load and back tension are selected for each case so one graduation of grid marked on the strip enters during each 5 minutes.

The isochromatic fringe pattern is photographed through a monochromatic filter of λ = 546.1 nm, and the isoclinic fringe pattern is recorded by using a colour film with a slightly over-exposure for separating the isoclinic fringe. The deformed grid on the strip is also recorded.

3.4 Experimental results

As an example of the results obtained, Fig. 29 shows the values of drawing load P_1 and back tension P_2 in relation to the ratio P_2/P_1. Figures 30 and 31 show the isochromatic and isoclinic (0°) fringe photographs in dark field for P_2/P_1 = 1/2. The isochromatic and isoclinic fringe patterns for P_2/P_1 = 0 and 1/2 are shown in Figs. 32 and 33. The fringe order in the roller specimen for P_2/P_1 = 1/2 is fairly reduced in comparison with that for P_2/P_1 = 0.

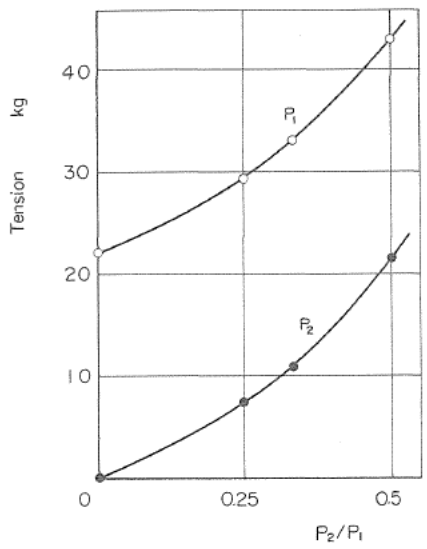

Fig. 29 Relation between drawing load P_1 and P_2 to the ratio P_2/P_1

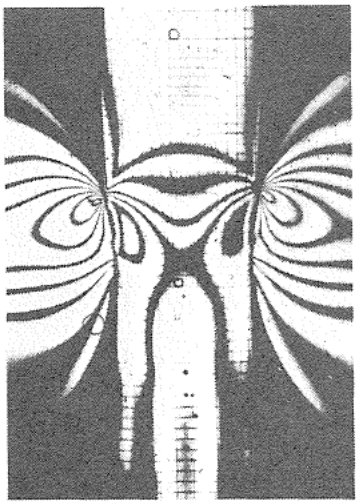

Fig. 30 Isochromatic fringe photograph (r = 15.5 percent, P_2/P_1 = 1/2)

Fig. 31 Isoclinic fringe photograph (r = 15.5 percent, P_2/P_1 = 1/2, 0°)

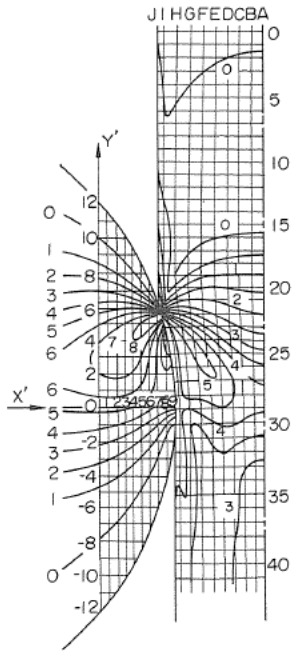

Fig. 32(a) Isochromatic fringe pattern
(r = 15.5 percent, $P_2/P_1 = 0$)

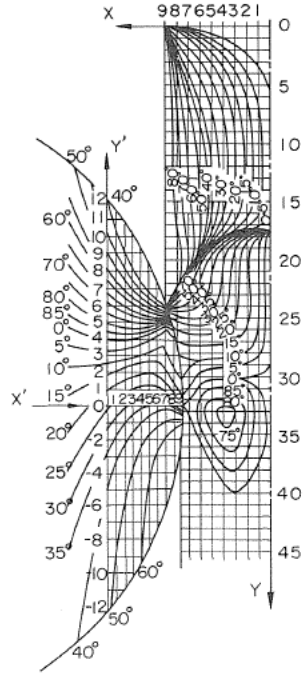

Fig. 32(b) Isoclinic fringe pattern
(r = 15.5 percent, $P_2/P_1 = 0$)

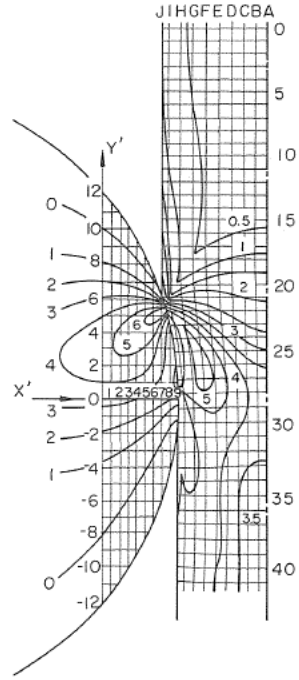

Fig. 33(a) Isochromatic fringe pattern
(r = 15.5 percent, $P_2/P_1 = 1/2$)

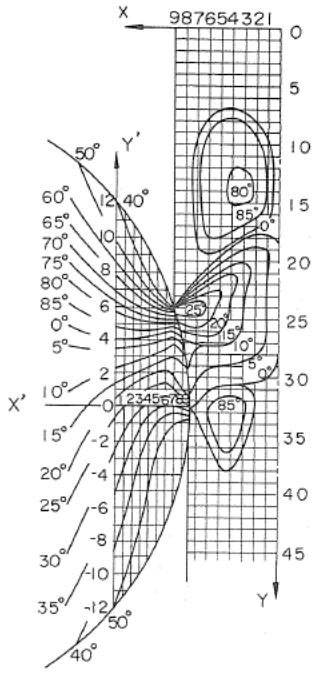

Fig. 33(b) Isoclinic fringe pattern
(r = 15.5 percent, $P_2/P_1 = 1/2$)

3.5 Stress distribution within specimens

In the above figures, the coordinate system $X'Y'$ established on the roller specimen is the same one as that shown in Fig. 14. In Figs. 32(b) and 33(b), the coordinate system XY is established on the strip specimen. The network which consists of the longitudinal lines A, B, ··· , J and the horizontal lines 1, 2, ··· , 40, ··· in Figs. 32(a) and 33(a) are deformed patterns of the square grid incised on the strip.

Figures 34 and 35 show the distribution of the principal stress difference within strip specimen for $P_2/P_1 = 0$ and 1/2. The coordinate system XY on the strip is the same one as that in Figs. 32(b) and 33(b). The principal stress difference has a minus sign with small magnitude within a part of strip just before the entrance of roller gap for $P_2/P_1 = 0$ (Fig. 34), while such a trend does not appear for $P_2/P_1 = 1/2$ (Fig. 35).

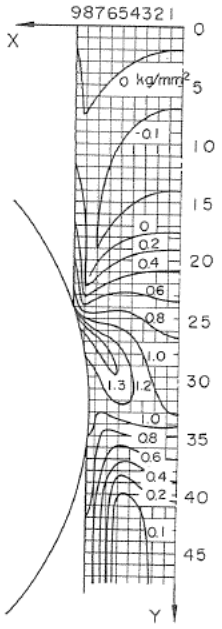

Fig. 34 Distribution of $\Delta\sigma$
(r = 15.5 percent, $P_2/P_1 = 0$)

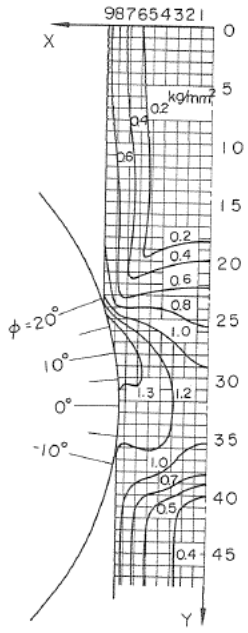

Fig. 35 Distribution of $\Delta\sigma$
(r = 15.5 percent, $P_2/P_1 = 1/2$)

The stress components were obtained by using the shear-difference method from the distribution of principal stress difference and the corresponding isoclinic pattern in the same way as mentioned previously. Figures 36 and 37 show, for example, the stress distributions in the sections $Y' = 0$, 2, 5 within the roller for $P_2/P_1 = 1/2$ and 0 with the open circles. The distribution of σ_y calculated separately along the sections passing through free boundary are entered with the solid circles. As found in these figures, the open and solid circles almost coincide with each other. In comparing Fig. 36 with Fig. 37, it is found that the stress in roller specimen is reduced significantly by the action of back tension.

Figure 38 shows the distributions of stress component, for $P_2/P_1 = 1/2$ along the sections $Y = 20$, 25, 32 and 42 in the strip, with the open circles. The solid circles show the corresponding value of σ_y calculated separately along the sections $X = 0$, 1, 2, ··· basing on the stress values in the section $Y = 15$. As found from the figure, the corresponding both values agree well with each other. Figure 39 shows the same results as shown in Fig. 38 for $P_2/P_1 = 0$, for comparison.

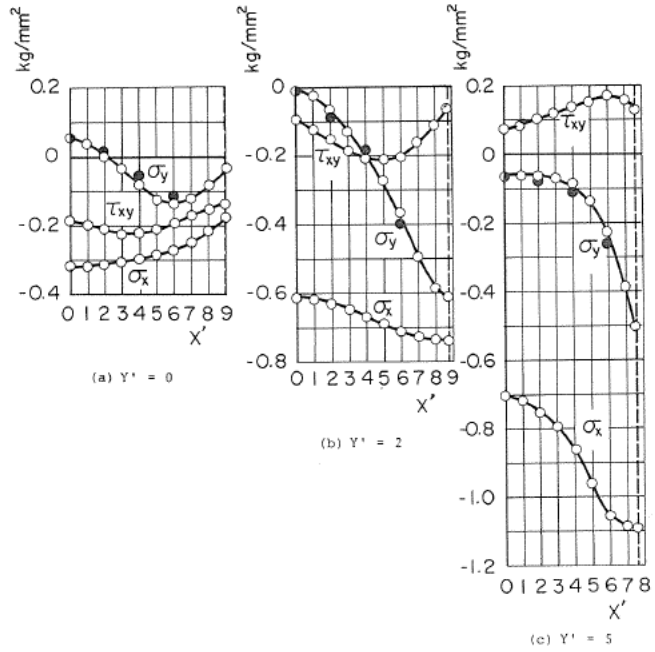

Fig. 36 Distribution of stress components within roller-dies ($P_2/P_1 = 1/2$)

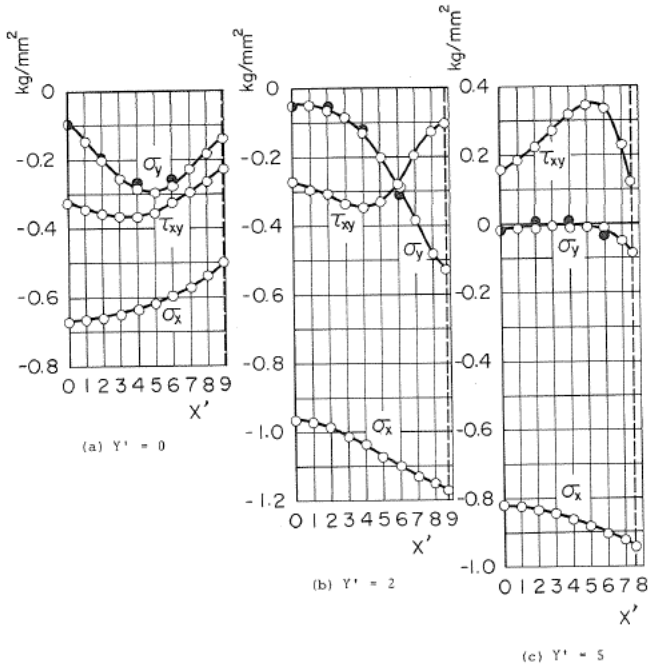

Fig. 37 Distribution of stress components within roller-dies ($P_2/P_1 = 0$)

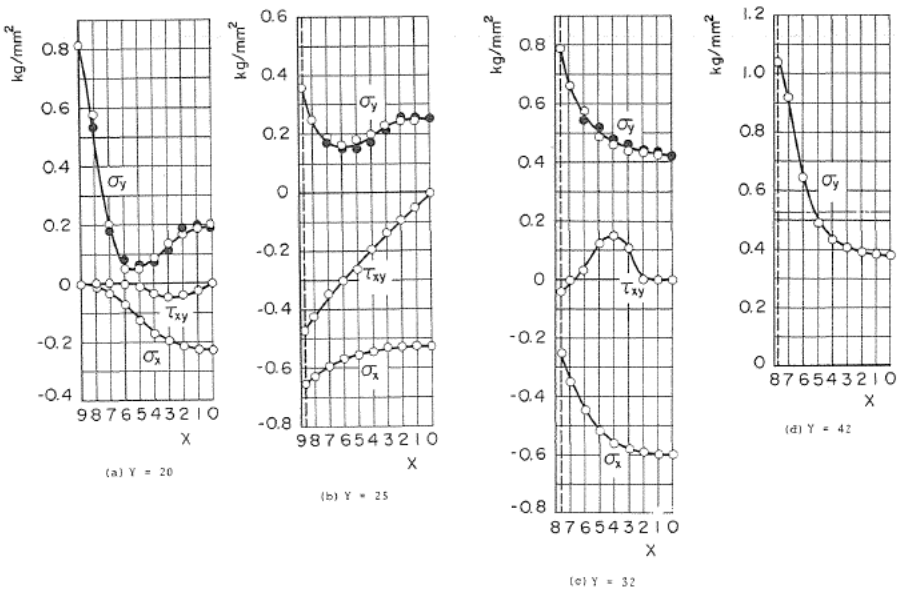

Fig. 38 Distribution of stress components within the strip ($P_2/P_1 = 1/2$)

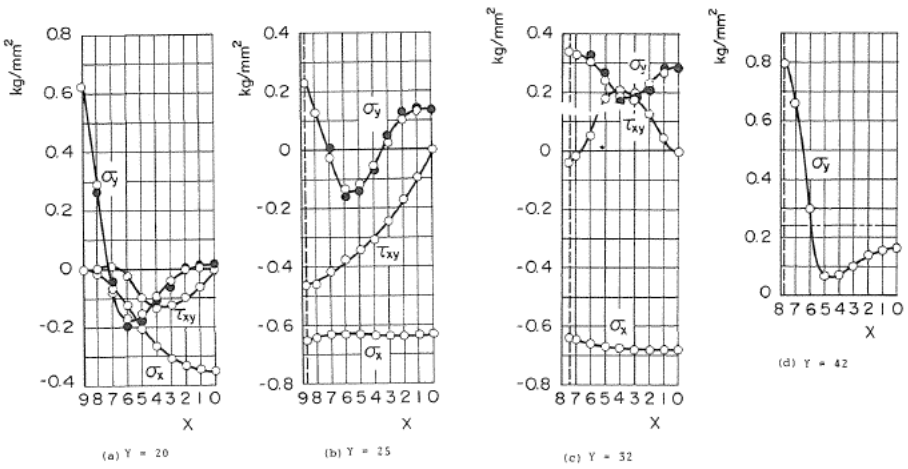

Fig. 39 Distribution of stress components within the strip ($P_2/P_1 = 0$)

Comparison between Figs. 38 and 39 shows a remarkable difference between the values of σ_y for $P_2/P_1 = 1/2$ and 0. The values of σ_x for $P_2/P_1 = 1/2$ and 0 also differ considerably. The value of τ_{xy} for $P_2/P_1 = 1/2$ is slightly lower than that for $P_2/P_1 = 0$. Thus, the stress state in the strip for $P_2/P_1 = 1/2$ may be regarded as that an axial stress is added to the stress state in the strip for $P_2/P_1 = 0$.

3.6 Stress distribution on the contact surface

Distributions of the contact pressure σ_n and the frictional shear stress τ_n on the contact surface are shown in Figs. 40 through 42 for P_2/P_1 = 0, 1/3 and 1/2 in relation to the value of ϕ shown in Fig. 35, in which the solid and dashed curves correspond to the values obtained on the strip and roller sides, respectively. As found from these figures, the corresponding values of σ_n obtained on both sides by means of the different methods agree well with each other. On the roller surface, the area surrounded by the horizontal coordinate axis and the plus part of the curve showing the distribution of τ_n is almost equal to that surrounded by the same axis and the minus part of the same curve, which shows that the resistance to the free rotation of the roller is negligible.

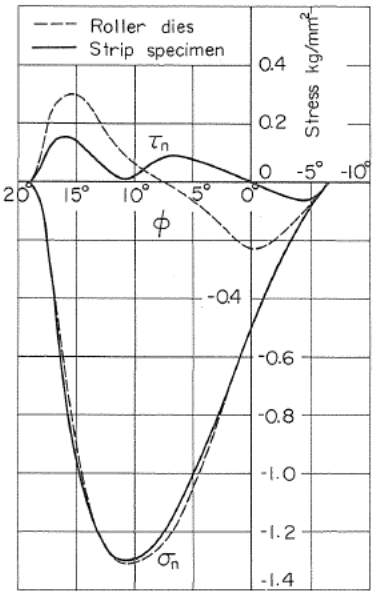

Fig. 40 Stress distribution on the contact surface ($P_2/P_1 = 0$)

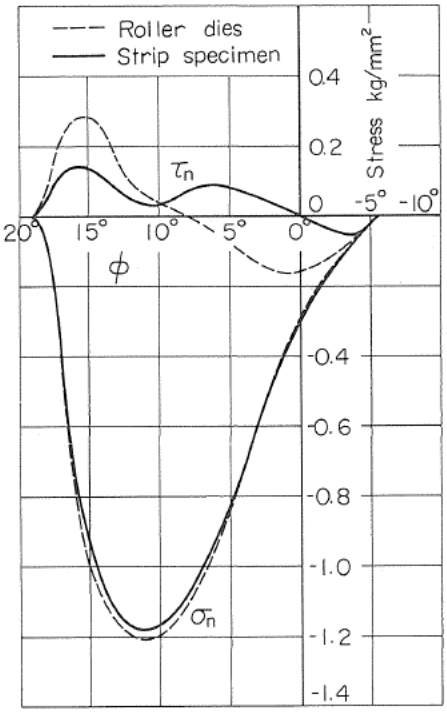

Fig. 41 Stress distribution on the contact surface ($P_2/P_1 = 1/3$)

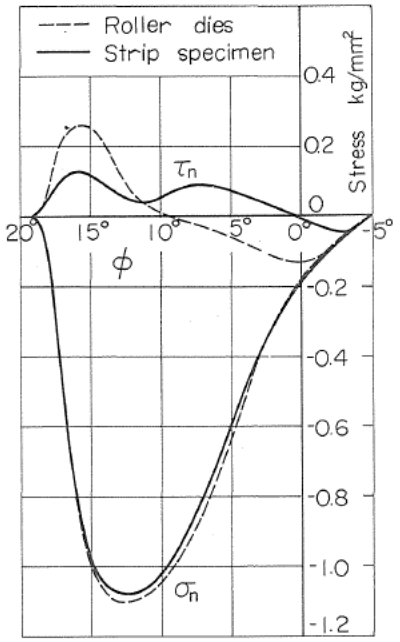

Fig. 42 Stress distribution on the contact surface ($P_2/P_1 = 1/2$)

3.7 Discussion

When the difference between the drawing load P_1 and the back tension P_2 and the sum of the components of σ_n and τ_n in the Y-direction on the contact surface are designated as A and B, respectively, A and B should be equal with each other. Table 5 showing the comparison of A and B in the cases of $P_2/P_1 = 0$, 1/3 and 1/2 indicates that the experimental errors are within 5 percent. The sum of σ_y over cross section should be equal to P_2 or P_1 for the section before the entrance or after the exit of the contact surface, and the results of experiment really satisfy these conditions within a few percent of errors. The effect of friction on the contact surface between the strip specimen and the glass plates is thus not so significant.

Table 5 Comparison of A and B

P_2/P_1	0	1/3	1/2
P_1 (kg)	22.00	33.00	43.00
P_2 (kg)	0	11.00	21.50
$A = P_1 - P_2$ (kg)	22.00	22.00	21.50
B (kg)	22.62	21.40	20.48
$\frac{A-B}{A} \times 100$ (%)	-2.82	2.73	4.74

As found from Figs. 40 through 42, the values of contact pressure σ_n on the contact surface obtained on the roller and strip sides agree well with each other. As regards the frictional shear stress τ_n on the contact surface, the difference between the distribution curves obtained on the roller and strip sides is due to the squeeze effect of oil film between contact surface away from the point of maximum contact pressure while the roller dies is rotating as an elastic body with a constant angular velocity and the strip is flowing plastically with varying velocity as a function of location. According to such an idea, the point where σ_n has its maximum value should coincide with the point of intersection of the solid and dashed curves showing τ_n. In these figures, the above-mentioned condition is really satisfied within small errors. It is found from Figs. 40 through 42 that the value of σ_n is remarkably reduced, especially in comparing the case of $P_2/P_1 = 1/2$ with that of $P_2/P_1 = 0$, as well as a fairly amount of reduction on the value of τ_n by the effect of back tension.

Moreover, the difference between the values of τ_n on the contact surfaces of roller and strip is also reduced considerably. The length of contact arc is shortened more or less with the effect of back tension, which may be due to a suppresion of elastic recovery after drawing by the back tension.

In such a way, the variation of stress distributions within roller-dies and strip by back tension, corresponding to the reduction of the resistance to drawing, may be analysed in detail.

At a sufficient distance after leaving the contact surface, the stress state within the strip may be found as of uniaxial tension from the corresponding isoclinic pattern. The difference between the distribution of σ_y and the mean value of σ_y may thus be regarded as a residual stress distribution, because the mean value of σ_y is reduced to zero after releasing the tension to the strip. For example, the double-dotted chain line in Figs. 38(d) and 39(d) show the mean value of σ_y, and thus the distribution of residual stress may be found by reducing the mean value to zero. Judging from these figures, any remarkable change of residual stress is not found with increase of back tension, but some trend may be recognized in the distribution of residual stress in the central part of the strip.

4. Strip Drawing Through Wedge-Shaped Dies[11]

Strip drawing through wedge-shaped dies is one of the typical example of plastic work. Stress analysis within the strip under plastic work has been performed by constructing the so-called slip-line field with an assumption of the rigid-plastic materials, and a good many results have been found by using this method.

This method is convenient to obtain a fairly good approximation by a simple calculation, but a suitable assumption for the analysis is necessary to obtain the precise analytic result. Moreover, it is important to get the informations what kind of phenomenon is arising in an actual plastic work in order to establish the suitable assumption. Any analytical result without such a suitable assumption should be unavailable for actual use.

The photo-rheologic stress analysis may be a powerful tool to offer the suitable informations on the actual plastic work.

4.1 Experimental apparatus

Figure 43 shows an outline of the experimental apparatus used, in which a softened celluloid strip is drawn by a dead-load with a constant speed through the wedge-shaped dies of a half-angle 5° made of Araldite plate. In order to obtain the plane strain state in the plastic deformation of strip, the strip is restricted on both sides by a pair of thick glass plates which are supported with ball bearings. The effect of friction on the contact surfaces between the glass plates and the strip is thus significantly reduced by a vertical movement of glass plates together with that of the strip.

Since the contact surface of glass plates is preliminary covered with oil film, the effect of friction on the contact surface to the relative movement due to local displacement of the strip may be considered to be small. When the apparatus is immersed in an oil bath filled with spindle oil heated at 65°C, the celluloid strip begins to flow plastically under external load while the Araldite dies remain in a glassy elastic state. As the mechanical property of celluloid is sensitive to temperature, the range of temperature distribution around the specimen and that of its variation during testing are kept within ± 0.05° C.

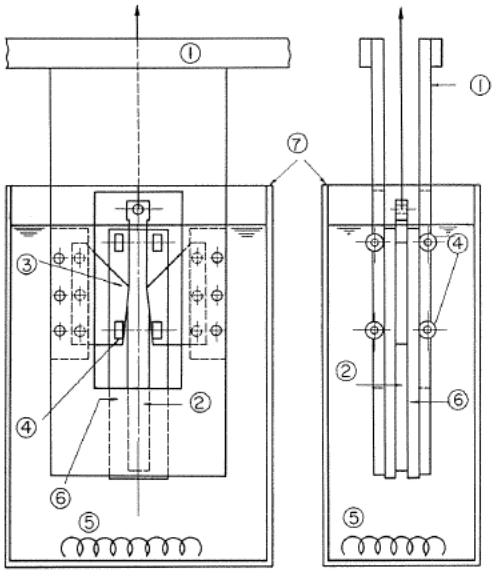

Fig. 43 Experimental apparatus

4.2 *Specimens and experimental procedure*

Die specimen was prepared from an Araldite plate of 6 mm thick without initial stress, and its contact surface with the strip was very smooth. As the result of calibration test at 65°C, its fringe stress value per unit thickness was found as 0.162 kg/mm². Strip specimen was prepared from a celluloid plate of 6 mm thick whose mechanical property was the same as that used for the experiments mentioned previously. Shapes and sizes of the specimens are shown in Fig. 44 and the inserted table. The guide part of strip was prepared so that the strip could contact closely with the die surface before drawing. A square grid of 1 mm distance was incised on the strip in order to trace each element during deformation.

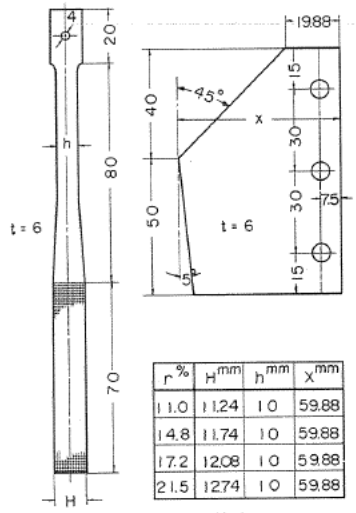

r %	H mm	h mm	X mm
11.0	11.24	10	59.88
14.8	11.74	10	59.88
17.2	12.08	10	59.88
21.5	12.74	10	59.88

Fig. 44 Shapes and sizes of specimens

As shown in Fig. 44, the narrowest clearance of the dies h, which corresponds to the strip width after drawing, was kept as h = 10 mm, and the reduction ratio of strip width $r = (H-h)/H$, where H denotes a strip width before drawing, was selected as r = 11.0, 14.8, 17.2 and 21.5 percent. Drawing load P was selected so that the strip could be drawn by one graduation of grid for each 5 minutes. In order to avoid a stick-slip action on the contact surface, the contact surface of strip specimen was covered with a thin film of polymer.

Isochromatic fringes within the specimens were photographed through a monochromatic filter of λ = 546.1 nm, and isoclinic fringes were recorded with the use of colour film by extinguishing isochromatic fringes at a slightly over-exposure. Deformation state of the square grid was also recorded for each instant.

4.3 *Experimental results*

As examples of the results obtained by the above-mentioned experiment, Figs. 45 and 46 show the photographs of isochromatic fringe in dark field and isoclinic fringe at 0° for r = 21.5 percent. Figures 47 and 48 show the isochromatic and isoclinic fringe patterns for r = 21.5 percent. A relation between the drawing load P and the reduction ratio r is shown in Fig. 49.

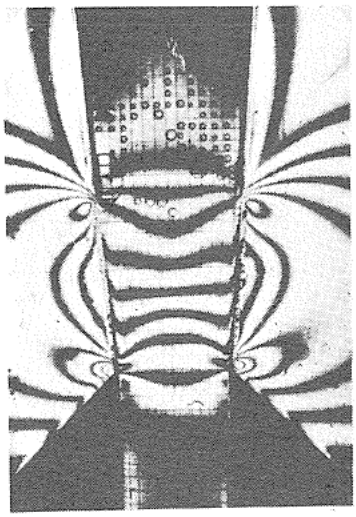

Fig. 45 Isochromatic fringe photograph (r = 21.5 percent, dark field)

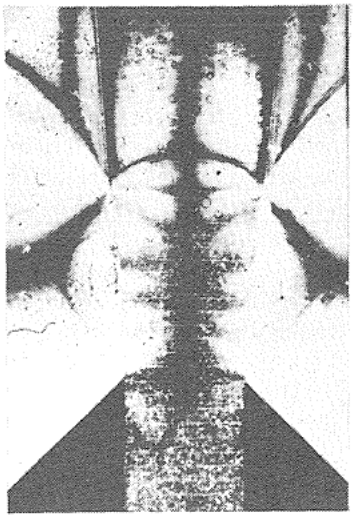

Fig. 46 Isoclinic fringe photograph (r = 21.5 percent, 0°)

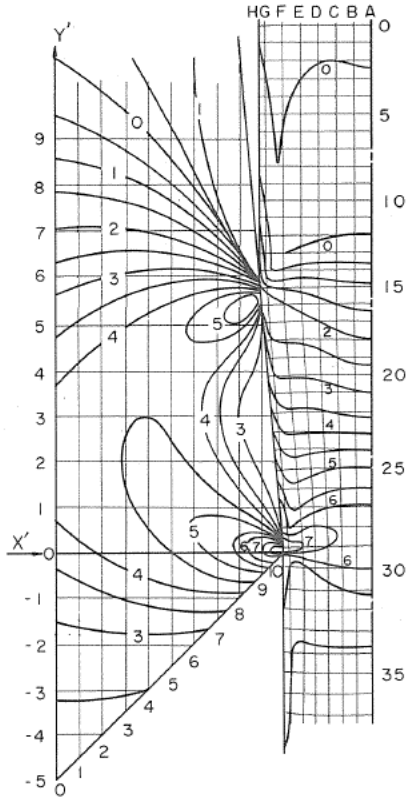

Fig. 47 Isochromatic fringe pattern (r = 21.5 percent)

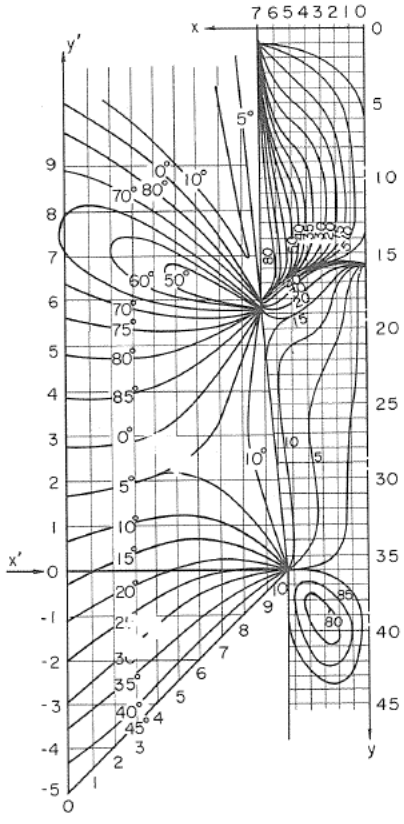

Fig. 48 Isoclinic fringe pattern (r = 21.5 percent)

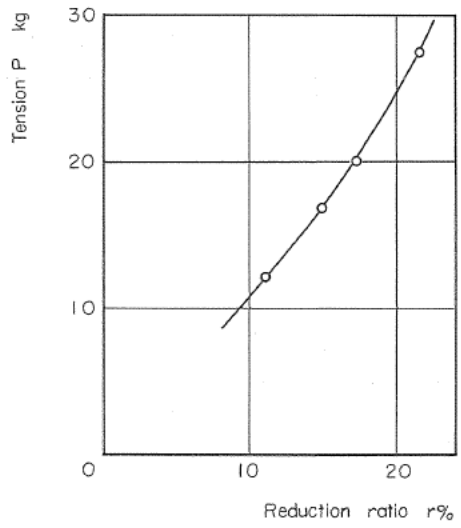

Fig. 49 Relation between the drawing load P and reduction-ratio r.

4.4 *Stress distribution in the dies*

As the die specimen remains in its elastic state, the stress distribution in the die was obtained by the usual method in photoelasticity. For this purpose, a coordinate system $x'y'$ was established on the die specimen (Fig. 48), in which the sections $x' = 0, 1, 2, \cdots, 10$ divided the horizontal axis into each $0.02X$ (X is the maximum width of die specimen, Fig. 44), and the sections $y' = -5, \cdots, -1, 0, 1, \cdots, 9$ divided the vertical axis into $0.04X$.

As an example of the results obtained, the open circles in Fig. 50 show the stress distributions in the sections $y' = 0$, 3 and 5 obtained by the shear-difference method along the sections parallel to x'-axis, starting from the stress values obtained beforehand on the sect-

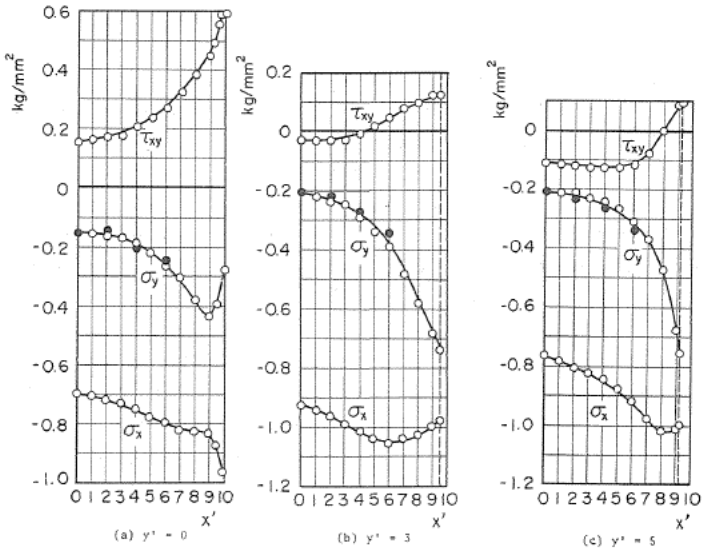

Fig. 50 Stress distributions within wedge-shaped dies (r = 21.5 percent)

circles in the figure show the value of σ_y obtained independently along the sections $x' = 0$, 2, 4 and 6 passing through the free surface of die specimen. The corresponding open and solid circles coincide well with each other.

4.5 *Distribution of principal stress difference in the strip*

The principal stress difference in the strip cannot be obtained directly from isochromatic fringe pattern, as mentioned previously. Thus, the principal stress difference was obtained by using the necessary relations mentioned previously together with the time rate of fringe order variation in each element identified by the grid on the specimen. As an example of the results, Fig. 51 show the distribution of the principal stress difference within the strip specimen for $r = 21.5$ percent.

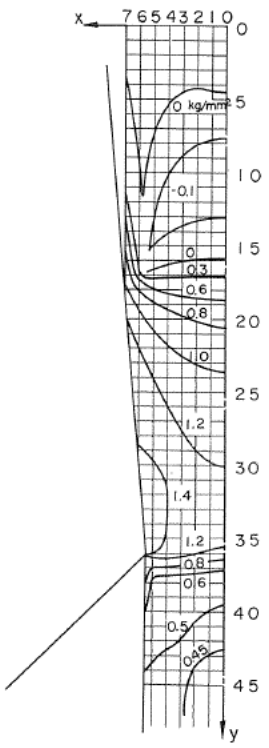

Fig. 51 Distribution of $\Delta\sigma$ within the strip (r = 21.5 percent)

4.6 *Stress distribution within the strip*

Stress distribution in the strip may be found by means of the shear-difference method by using the distribution of principal stress difference together with the isoclinic fringe pattern. For this purpose, as shown in Figs. 48 and 51, a coordinate system xy was established on the strip, in which the sections $x = 0, 1, \cdots, 7$ divided a half-width of the strip into 7 parts equally, and the sections $y = 0, 1, 2, \cdots$ divided a longitudinal axis into the same distance. The stress components were obtained first on the section $y = 0$ passing through free surface of the strip, and the distribution of these components along $x = 0$ were obtained. Star ting from the latter values, the stress distributions were obtained in each section parallel to x-axis passing through the contact surface. As an example of the results obtained, Fig. 52 shows the stress distributions on the sections $y = 13$, 20, 30 and 45 with the open circles. As shown in Fig. 48, the sections $y = 13$ and 45 pass through the free surface of strip, and thus the stress distribution may be found directly. Moreover, as found from Fig. 48, the stress state in the section $y = 45$ is a uniaxial one. The solid circles in Fig. 52 show the value of σ_y obtained in the y-direction starting from the stress values on the section $y = 10$, which agree well with the corresponding open circles.

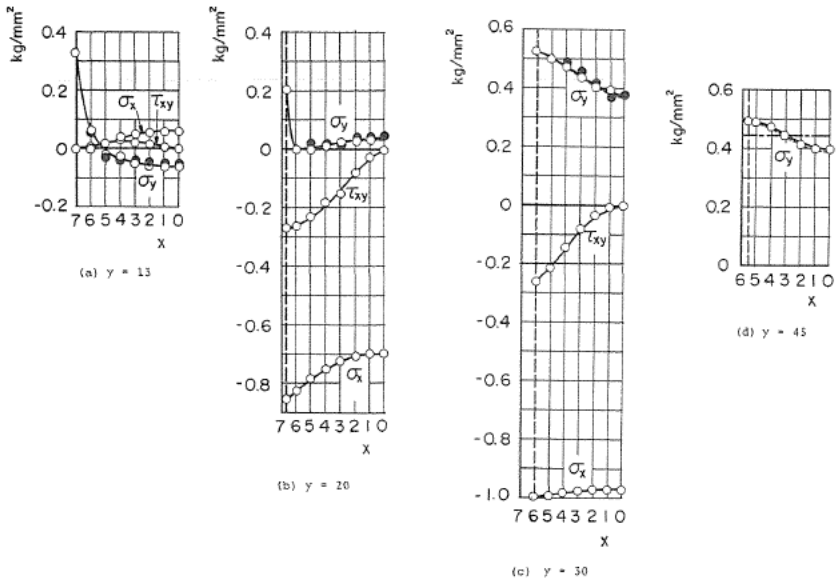

Fig. 52 Stress distributions within the strip (r = 21.5 percent)

4.7 Stress distribution on the contact surface

Stress discribution on the contact surface may be found from the above obtained result. The distribution of contact pressure σ_n and the frictional shear stress τ_n may thus be found from them by a rotation of coordinate system on the contact surface.

As an example, the solid curves in Figs. 53 through 56 show the distributions of σ_n and τ_n on the contact surface of the strip for each value of r. The maximum value of σ_n appears near the exit of the die for every value of r, which almost remains unchanged for r = 11 and

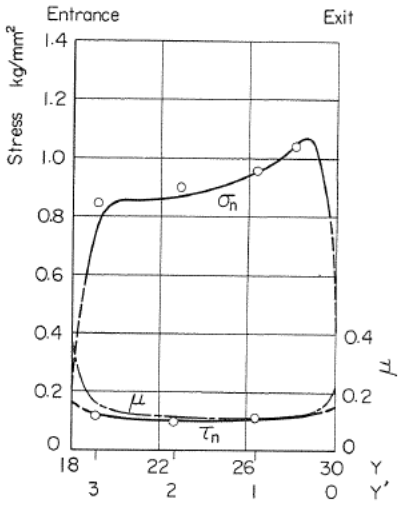

Fig. 53 Stress distribution on the contact surface (r = 11 percent)

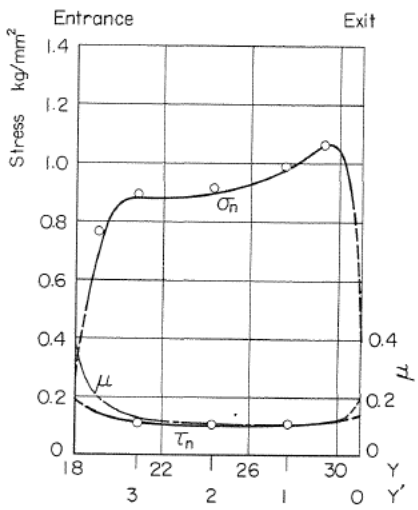

Fig. 54 Stress distribution on the contact surface (r = 14.8 percent)

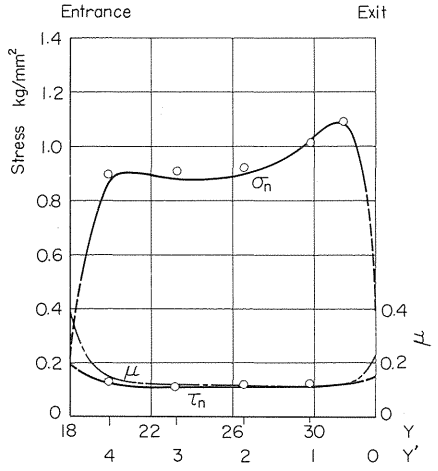

Fig. 55 Stress distribution on the contact surface (r = 17.2 percent)

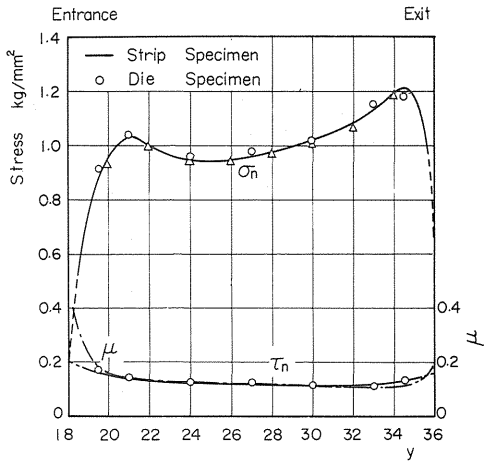

Fig. 56 Stress distribution on the contact surface (r = 21.5 percent)

14.8 percent. For the value of r larger than them, another maximum value appears near the entrance of the die and the former maximum value also begins to grow. The transition of the value of σ_n between both maximum forms a distinct hollow for large value of r.

The distribution of τ_n over contact surface is almost uniform except a slight increase near both ends and is kept almost unchanged for every value of r.

The open circles in these figures show the values of σ_n and τ_n on the contact surface of the die, which agree well with the corresponding values obtained on the strip side.

4.8 Discussion and conclusion

The corresponding open and solid circles showing the values of σ_n obtained independently along the different paths in Figs. 50 and 52 agree with each other, which shows the high accuracy of the results of the shear-difference method.

In Figs. 53 through 56, the open circles showing σ_n obtained on the die side lie with sufficient accuracy on the curve showing the corresponding values obtained on the strip side. This means that the normal stress components on the contact surface satisfy the condition of continuity. The accuracy of the result obtained by the photo-rheologic stress analysis may thus be considered to have an accuracy of the same order as that obtained by photoelasticity.

The ratio τ_n/σ_n may be regarded as an equivalent frictional coefficient of Coulomb type μ, and its distributions are entered in these figures with the chain curves. Strictly speaking, these distributions are not always uniform over contact surface because some increases appear near both ends and a slight decrease is recognized toward exit. However, these may be regarded almost constant as a whole except near both ends, which enables us to assume the state of Coulomb friction.

The sum of σ_y on any section of the strip passing through contact surface should be equal to the difference between the drawing load P and the sum of the components of σ_n and τ_n in the y-direction on the contact surface in the range from that section to the exit. By designating the former and the latter value as A and B, errors in agreement of A and B for $r = 21.5$ percent have been examined as shown in Table 6, which shows that A and B agree within a few percent

of errors.

Table 6 Comparison of A and B

Section y	21	24	28	32	35
A (kg)	3.6	9.2	16.8	22.8	26.0
B (kg)	3.8	8.8	15.9	21.7	26.1
$\frac{A-B}{B} \times 100$ (%)	-5.6	4.3	5.4	4.8	-0.4

The sum of σ_y on each section of the strip is equal to zero before coming into contact with the die or to the drawing load P after leaving the contact surface. Each condition is satisfied in the experimental results with a sufficient accuracy.

Since the sum of σ_y on each section after the exit of die becomes to zero after releasing the drawing load, the difference between the distribution of σ_y and its average value in each section is equivalent to a distribution of the residual stress after drawing. Since the chain line in Fig. 52 (d) shows, for example, an average value of σ_y, if the average value is regarded as zero, the distributions of residual stress after drawing may be found from the figure.

The thin dashed curve in Fig. 52 as well as the small triangles in Fig. 56 show the results obtained by using a constant principal stress ratio ($\sigma_1/\sigma_2 = -1$) as the first approximation, while the above-mentioned results have been obtained in considering the effect of principal stress ratio for precise estimation. As found from these figures, the differences between the improved results and their first approximations are not so significant, which shows the effort for obtaining the precise estimation of stress distirbution is little rewarded.

Conclusion

In the present paper, fundamental concept and experimental procedure of the photo-rheologic stress analysis proposed by the author are described in detail.

Some examples performed by this method show that the experimental stress analysis on the plastically flowing body is made possible by means of the method and a variety of interesting results may be obtained in the unknown field of practical importance.

References

1) Y. Ohashi; Brit. J. Appl. Phys., Vol. 6 (1965), 985
2) Y. Ohashi and T. Nishitani; Bulletin of JSME, 9-34 (May, 1966), 245
3) И.И. Бугаков: Исследования по упругости и пластичности, том. 1 (1961), 107 Изд. Ленингладского Университета
4) Y. Ohashi, T. Nishitani and M. Ishida; J. Strain Analysis, 6-4(1971), 250
5) M.M. Frocht and Y.F. Cheng; Trans. ASME, Ser.E, 29-1 (March, 1962), 1
6) Y. Ohashi, M. Tokuda and H. Tobushi; Bulletin of the JSME, 16-92 (Feb., 1973), 194
7) А.А. Ильюшин: Вопросы теории пластичности, (1961), Изд. АН СССР, 3
8) Y. Ohashi, S. Murakami and M. Suzuki; J. Phy. D: Appl. Phys., Vol. 5 (1972), 2129
9) Y. Ohashi and T. Nishitani; Int. J. Mech. Sci., Vol. 9 (1967), 359
10) Y. Ohashi and T. Nishitani; Trans. JSME, 33-256 (Dec., 1967), 1932 (in Japanese)
11) Й. Оохаси и Т. Нишитани: Инж. Ж., Мех. Твер. Тела, том. 5 (1968), 115